JOURNAL OF COMPUTATIONAL PHYSICS **123,** 311–329 (1996)
ARTICLE NO. 0026

Stability Analysis of Operator Splitting for Large-Scale Ocean Modeling

ROBERT L. HIGDON* AND ANDREW F. BENNETT†

*Department of Mathematics, Oregon State University, Corvallis, Oregon 97331-4605; †College of Oceanic and Atmospheric Sciences, Oregon State University, Corvallis, Oregon 97331-5503

Received February 8,1994; revised June 12, 1995

The ocean plays a crucial role in the earth's climate system, and an improved understanding of that role will be aided greatly by high-resolution simulations of global ocean circulation over periods of many years. For such simulations the computational requirements are extremely demanding and maximum efficiency is essential. However, the governing equations typically used for ocean modeling admit wave velocities having widely varying magnitudes, and this situation can create serious problems with the efficiency of numerical algorithms. One common approach to resolving these problems is to split the fast and slow dynamics into separate subproblems. The fast motions are nearly independent of depth, and it is natural to try to model these motions with a two-dimensional system of equations. These fast equations could be solved with an implicit time discretization or with an explicit method with short time steps. The slow motions would then be modeled with a three-dimensional system that is solved explicitly with long time steps that are determined by the slow wave speeds. However, if the splitting is inexact, then the equations that model the slow motions might actually contain some fast components, so the stability of explicit algorithms for the slow equations could come into doubt. In this paper we discuss some general features of the operator splitting problem, and we then describe an example of such a splitting and show that instability can arise in that case.

1. INTRODUCTION

In this paper we examine some stability problems that can arise when operator splittings are used to compute numerical solutions of systems of partial differential equations that describe large-scale oceanic flows. Such systems admit solutions that vary on different time scales, and for the sake of efficiency it is desirable to compute the fast and slow parts of the solution separately. However, if the splitting is inexact, then unstable behavior could be displayed by the computational algorithm.

One motivation for performing such computations is that the ocean is an important component of the earth's climate system, and a better understanding of climate will be aided greatly by high-resolution computer simulations of global ocean circulation over periods of decades or centuries. An example of the ocean's role is the transport of heat energy due to mechanisms such as north–south boundary currents and mixing due to eddies that are shed from ocean currents (Robinson [18]). In middle latitudes, oceanic eddies typically have widths on the order of 200 to 300 km. However, eddies in the higher latitudes typically have widths of about 50 km or even less, and boundary currents can have widths of roughly this magnitude. A numerical model that resolves such features over long times will thus pose some very large computational demands.

In such a model, the most straightforward time discretization would be an explicit method. However, such a method would suffer from a severe restriction on the allowable time step, due to the nature of the wave motions that are typically found in large-scale models of ocean circulation. In existing models it is commonplace to eliminate sound waves by various means. The remaining dynamics then include several classes of waves; prominent among these are external gravity waves (i.e., surface gravity waves) and internal gravity waves. External motions are approximately independent of depth, whereas internal waves can be regarded as undulations in surfaces of constant density within the fluid. The speed of the external gravity waves is approximately $\sqrt{gH}$, where g is the acceleration due to gravity, and H is the depth. In the deep ocean, the speed of external gravity waves is on the order of 200 m/s. On the other hand, the speed of internal waves is on the order of 1 or 2 m/s or slower; particle velocities are typically of at most this magnitude. If one uses an explicit finite difference method to solve a system that admits both external gravity waves and internal gravity waves, then the permissible time step is about two orders of magnitude smaller than would be the case if the fast waves were not present. The high computational cost of such an explicit method makes it highly desirable to employ a different kind of time discretization.

One such alternative is to split the fast and slow motions into separate subproblems. The fast external motions are essentially two-dimensional, due to the approximate inde-

0021-9991/96 $18.00

pendence from depth. One is then tempted to seek a splitting in which the external motions are modelled by a two-dimensional set of equations, and the slow internal motions are modelled by a three-dimensional system. The fast, two-dimensional equations could be solved either with an implicit method with long time steps or with an explicit method with short time steps that are determined by the fast waves. The larger three-dimensional system could then be solved with an explicit method having long time steps that are determined by the slow wave speeds. However, if the split is inexact, then the equations that model the slow motions might actually admit fast motions, in some sense. In that case, instabilities could arise if long time steps are used to advance those equations in time. In this paper we discuss some general aspects of the operator splitting problem, and we then describe the nature of the instability in one representative ocean model.

The idea of operator splitting has been incorporated into several computational models of ocean circulation. In the examples described below, the velocity field for the two-dimensional fast equations is obtained from a vertical average of the horizontal velocity field in the original three-dimensional system. This procedure is motivated by the approximate depth independence of the horizontal velocity field in external wave motions. In each of the examples described here, the underlying governing equations are the hydrostatic Euler equations, or ''primitive'' equations.

One of the earliest and most widely used ocean models is one developed by Bryan and Cox and subsequently modified by several researchers. See, e.g., Bryan [4], Cox [5], Semtner and Chervin [19, 20], and Smith, Dukowicz, and Malone [21]. In this class of models, the free-surface boundary condition at the top of the fluid is replaced by a ''rigid lid'' boundary condition, in which the upper surface is level and the vertical component of velocity is required to be zero along that surface. The rigid-lid approximation has the effect of making the external gravity wave speed infinite, and the fast portion of the solution is modeled by a two-dimensional elliptic equation that is solved at each long time step. In these models the vertical coordinate is a linear height z.

In recent years several models have been developed that use a free-surface condition instead of a rigid lid. Killworth *et al.* [11] and Dukowicz and Smith [7] developed free-surface versions of the Bryan–Cox model; in [11] the fast two-dimensional equations are solved explicitly with a short time step, and in [7] these equations are solved implicitly with a long time step. Blumberg and Mellor [3] developed a free-surface model in which the vertical coordinate is a quantity σ that represents the proportional height relative to the bottom and top of the ocean. Bleck and Smith [2] developed an ''isopycnal'' free-surface model in which the vertical coordinate is the reciprocal of density, or specific volume α. Another isopycnal free-surface model by Oberhuber [13] does not rely on an operator splitting, but instead it uses an implicit time discretization.

To one degree or another, the operator splittings described above are inexact. In the case of a linearized flow with a horizontal bottom, one can develop a model decomposition of the solution via separation of variables. See, e.g., Section 6.11 of Gill [9] and Section 2 of the present paper. In a rigid-lid model with vertical coordinate z, one type of solution is exactly independent of depth, and this corresponds to external motions. For this mode, the horizontal velocity field is exactly equal to the vertically averaged velocity described earlier. However, in real dynamics the fast and slow motions can be mixed due to such factors as variable bottom elevation and nonlinearity. In a free-surface model, the external mode varies slightly with depth; in such a model, a splitting based on depth averages can be inexact, even in the linearized case. Killworth *et al.* [11] reported some unstable behavior in their experiments, and they speculated that the problem may be due to inexact modal splitting. Each of the ocean models described earlier uses dissipation in the governing equations and/or smoothing with respect to time in order to suppress the growth of nonlinear instabilities. In practice, these mechanisms might also suppress some effects of inexact operator splitting.

In the present paper we discuss these issues in the context of isopycnal ocean modeling. In particular, we describe the operator splitting that was developed by Bleck and Smith [2] for isopycnal coordinates, and we show that this splitting can yield unstable algorithms in the linearized case. We are not aware of any other published operator splittings for the primitive equations in this coordinate system.

We focus on isopycnal coordinates because of their appeal on physical grounds. In such a coordinate system, fluid moves approximately along surfaces corresponding to constant values of the vertical coordinate, so water masses are tracked automatically by the choice of coordinate system. A uniform discretization in the vertical coordinate is not uniform with respect to z; in this sense the grid is adaptive in the vertical direction. Finally, in ocean modeling it is standard practice to introduce numerical diffusion in order to control the growth of nonlinear instabilities. In that event, the direction of diffusion should preferably be tangent to isopycnal surfaces so as not to mask cross-isopycnal diffusion processes that are sutble yet important (Redi [16], de Szoeke and Bennett [6]). This can be done most conveniently in an isopycnal setting.

In Sections 2.1 and 2.2 we summarize some properties of the primitive equations in isopycnal coordinates, and in Section 2.3 we describe the operator splitting that was introduced by Bleck and Smith for this system. In Section 3 we specialize this splitting to a linearized flow in one horizontal dimension with two fluid layers and a flat lower

boundary. In Section 4 we formulate a computational algorithm based on a simple time stepping scheme for the slow equations that would be nondissipative and stable if all of the fast variables were identically zero. In this formulation we also assume that the fast equations are solved exactly with respect to t. We make these choices so that there are no mechanisms to mask or aggravate any destabilizing effects of the operator splitting. We then show that the algorithm for the full system is unstable. In Section 5 we consider some alternative methods for solving the slow equations, including two predictor–corrector methods. These methods also show instability, although a correction step can reduce the rate of unstable growth. In Section 6 we describe the results of some numerical computations that confirm the preceding analysis. A summary is given in Section 7.

2. THE SYSTEM OF EQUATIONS

In Section 2.1 we describe the hydrostatic Euler equations, or primitive equations, for the case of isopycnal coordinates. In Section 2.2 we outline the modal structure of a linearized version of that system. This structure suggests how one might try to split the fast and slow dynamics of the primitive equations into separate subproblems. However, we also indicate how the split could be inexact in practical computations, so that stability can be a concern even in the linear case. In Section 2.3 we outline the operator splitting developed by Bleck and Smith [2].

2.1. *Primitive Equations in Isopycnal Coordinates*

Here we state the primitive equations in terms of coordinates (x, y, α, t), where α is the specific volume, or reciprocal of density. We assume that α is a strictly increasing function of z, so that α can be used as a vertical coordinate. It is then possible to write z in the form $z(x, y, \alpha, t)$; for fixed α and t, the graph of $z(x, y, \alpha, t)$ as a function of (x, y) represents a surface of constant density in the fluid.

Let $u(x, y, \alpha, t)$ and $v(x, y, \alpha, t)$ denote the components of fluid velocity in the x and y directions, respectively, and let $p(x, y, \alpha, t)$ denote the pressure. We consider the primitive equations in the form

$$u_t + uu_x + vu_y - fv = -M_x \tag{2.1a}$$

$$v_t + uv_x + vv_y + fu = -M_y \tag{2.1b}$$

$$M_\alpha = p \tag{2.1c}$$

$$p_{\alpha t} + (p_\alpha u)_x + (p_\alpha v)_y = 0, \tag{2.1d}$$

where

$$M(x, y, \alpha, t) = \alpha p(x, y, \alpha, t) + gz(x, y, \alpha, t) \tag{2.1e}$$

is the Montgomery potential and f is the Coriolis parameter. For a derivation, see, e.g., Eliassen and Kleinschmidt [8] or Haltiner and Williams [10].

Equation (2.1c) is based on an assumption that the fluid is in hydrostatic balance; that is, $p_z = -g\alpha^{-1}$, or $p_\alpha = -g\alpha^{-1}z_\alpha$. This assumption is equivalent to saying that the vertical component of particle acceleration is negligible, and it is an accurate approximation for flows in which the depth is small relative to the horizontal length scale (Gill [9]).

In the system (2.1), it is assumed that $\varpi = D\alpha/Dt = 0$, so that the specific volume of each fluid particle remains constant with time. This is equivalent to assuming that fluid particles flow along surfaces of constant density, which is a conventional approximation for large-scale oceanic flows. A more accurate approximation is to say that fluid particles flow along surfaces of constant entropy (Gill [9], Phillips [15]), so entropy would be an attractive vertical coordinate. However, this distinction is immaterial to the present discussion of numerical stability, and the present setting is simpler. If one did not assume $\varpi = 0$, then the terms ϖu_α, ϖv_α, and $(p_\alpha \varpi)_\alpha$ would appear on the left sides of (2.1a), (2.1b), and (2.1d), respectively.

In the horizontal momentum equations (2.1a), (2.1b) the gradient of $M = \alpha p + gz$ represents the horizontal forcing due to pressure. In the present coordinate system, the gradient of $p(x, y, \alpha, t)$ with respect to (x, y) would not represent the forcing correctly, as this gradient consists of derivatives for fixed α. Surfaces of fixed α are generally not horizontal, so p_x and p_y include vertical contributions, and a hydrostatic correction is then necessary. This correction is included in the quantities M_x and M_y.

In Eq. (2.1d), the quantity p_α indicates the thicknesses of layers bounded by surfaces of constant density; here, thicknesses are measured by the pressure differences across layers. Equation (2.1d) expresses changes in layer thickness in terms of horizontal mass flux.

2.2. *External and Internal Modes in the Linearized System*

We now describe the modal structure of solutions of a linearization of the primitive equation system (2.1). One such mode is the external mode, and the others are internal modes. Solutions of the linearized system do not exhibit all of the features of solutions of the nonlinear system (2.1), but a description of the external and internal modes in the linearized case can indicate some of the issues that are involved in splitting fast and slow dynamics into separate subsystems.

We consider solutions of (2.1) that are small perturbations of a static state for which $u = v = 0$, $z = \tilde{z}(\alpha)$, the pressure is $\tilde{p}(\alpha)$, and the Montgomery potential is $\tilde{M}(\alpha) = \alpha\tilde{p}(\alpha) + g\tilde{z}(\alpha)$. We also assume that f is constant.

For purposes of separating variables, suppose $\alpha_{\text{bot}} \le \alpha \le \alpha_{\text{top}}$, where α_{bot} and α_{top} are independent of (x, y, t). This assumption implies that the top and bottom of the fluid are surfaces of constant density. In the static solution mentioned above, these surfaces are horizontal, due to the condition $z = \tilde{z}(\alpha)$. This implies that the bottom of the fluid must be planar and level in the present linearized model.

For solutions that are small perturbations of the static state, we denote the pressure by $\tilde{p}(\alpha) + p(x, y, \alpha, t)$ and the Montgomery potential by $\tilde{M}(\alpha) + M(x, y, \alpha, t)$. That is, in the present discussion p and M will not denote pressure and Montgomery potential, respectively, but instead they will denote perturbations in those quantities. The system (2.1) is then approximated by the linear system

$$u_t - fv = -M_x \tag{2.2a}$$

$$v_t + fu = -M_y \tag{2.2b}$$

$$M_\alpha = p \tag{2.2c}$$

$$p_{\alpha t} + \tilde{p}_\alpha(\alpha)(u_x + v_y) = 0. \tag{2.2d}$$

At the top of the fluid the pressure is assumed to be equal to a constant value of atmospheric pressure, so the perturbation p in pressure must satisfy the boundary condition

$$p = 0 \quad \text{if } \alpha = \alpha_{\text{top}}. \tag{2.3a}$$

At the bottom of the fluid, we have $z(x, y, \alpha_{\text{bot}}, t) = \tilde{z}(\alpha_{\text{bot}})$, so the perturbation in z is zero when $\alpha = \alpha_{\text{bot}}$. The perturbations in the pressure and Montgomery potential must then satisfy

$$M = \alpha p = \alpha M_\alpha \quad \text{if } \alpha = \alpha_{\text{bot}}. \tag{2.3b}$$

Now use the method of separation of variables to construct solutions of the system (2.2) with boundary conditions (2.3). If functions of the form $u(x, y, \alpha, t) = \hat{u}(x, y, t)\phi(\alpha)$, $v(x, y, \alpha, t) = \hat{v}(x, y, t)\phi(\alpha)$, and $M(x, y, \alpha, t) = \hat{M}(x, y, t)\phi(\alpha)$ are inserted into (2.2), one obtains

$$\begin{aligned} \hat{u}_t - f\hat{v} &= -\hat{M}_x \\ \hat{v}_t + f\hat{u} &= -\hat{M}_y \\ \hat{M}_t + (1/\lambda)(\hat{u}_x + \hat{v}_y) &= 0, \end{aligned} \tag{2.4}$$

where λ and ϕ satisfy

$$\phi_{\alpha\alpha}(\alpha) = \lambda\tilde{p}_\alpha(\alpha)\phi(\alpha) \quad \text{for } \alpha_{\text{bot}} \le \alpha \le \alpha_{\text{top}} \tag{2.5a}$$

$$\phi_\alpha = 0 \quad \text{for } \alpha = \alpha_{\text{top}} \tag{2.5b}$$

$$\phi = \alpha\phi_\alpha \quad \text{for } \alpha = \alpha_{\text{bot}}. \tag{2.5c}$$

The eigenvalue problem (2.5) is a regular Sturm–Liouville problem (Morse and Feshbach [12]). The problem admits an infinite sequence of eigenvalues $\lambda_0, \lambda_1, \ldots$, with a complete set of corresponding eigenfunctions $\phi^{(0)}, \phi^{(1)}, \ldots$. Each eigenvalue λ_j is positive, since $\tilde{p}_\alpha < 0$, and we can label the eigenvalues so that $0 < \lambda_0 < \lambda_1 < \ldots$ with $\lambda_j \to \infty$ as $j \to \infty$. The eigenfunctions are orthogonal with respect to the weight function $\tilde{p}_\alpha(\alpha)$.

General solutions of the linearized system (2.2) can be expressed in terms of these eigenfunctions. For example, one can write

$$u(x, y, \alpha, t) = \sum_{j=0}^{\infty} \hat{u}^{(j)}(x, y, t)\phi^{(j)}(\alpha),$$

where

$$\hat{u}^{(j)}(x, y, t) = \frac{\int_{\alpha_{\text{bot}}}^{\alpha_{\text{top}}} u(x, y, \alpha, t)\phi^{(j)}(\alpha)\tilde{p}_\alpha(\alpha)\, d\alpha}{\int_{\alpha_{\text{bot}}}^{\alpha_{\text{top}}} (\phi^{(j)}(\alpha))^2\tilde{p}_\alpha(\alpha)\, d\alpha}. \tag{2.6}$$

Analogous representations apply to v and M, and the relation $M_\alpha = p$ then yields an expansion for p.

Each set of coefficients $\{\hat{u}^{(j)}, \hat{v}^{(j)}, \hat{M}^{(j)}\}$ satisfies the system (2.4), with $\lambda = \lambda_j$. This system has the structure of the linearized shallow water equations (e.g., Pedlosky [14]), with the constant $1/\lambda_j$ playing the role of the square of the wave speed. We will therefore write λ_j in the form $\lambda_j = 1/c_j^2$, with $c_j > 0$. The largest wave speed out of all of the modes is then c_0, and $c_j \to 0$ as $j \to \infty$. Estimates of c_0, c_1, ..., are given, e.g., by Bennett [1].

Of particular interest in the present paper is the problem of characterizing the fastest motions in the system and splitting these motions into a separate subproblem. Accordingly, we now examine the structure of the eigenfunction $\phi^{(0)}$ that corresponds to the smallest eigenvalue λ_0 and thus the largest wave speed c_0.

Suppose that a function ϕ satisfies the differential equation (2.5a), $\phi_{\alpha\alpha}(\alpha) = \lambda\tilde{p}_\alpha(\alpha)\phi(\alpha)$, with $\lambda > 0$. Since $\tilde{p}_\alpha(\alpha) < 0$, $\phi_{\alpha\alpha}$ and ϕ must have opposite signs. Suppose, without loss of generality, that $\phi(\alpha_{\text{top}}) > 0$. The boundary condition (2.5b) implies $\phi_\alpha(\alpha_{\text{top}}) = 0$; as α is decreased from α_{top}, the derivative ϕ_α must then become positive. When α reaches α_{bot}, ϕ must satisfy the boundary condition (2.5c), which states that the tangent line to ϕ must coincide with the line through the origin and the point $(\alpha_{\text{bot}}, \phi(\alpha_{\text{bot}}))$. If λ is equal to the smallest possible eigenvalue λ_0, then the concavity of the eigenfunction ϕ maintains a constant sign, ϕ and ϕ_α remain positive, and the largest value of ϕ_α is found when $\alpha = \alpha_{\text{bot}}$. However, for larger eigenvalues λ, the magnitude of $\phi_{\alpha\alpha}$ is larger relative to ϕ, so the graph of ϕ has larger curvature and undergoes oscillations.

We now estimate the extent to which $\phi^{(0)}(\alpha)$ varies for $\alpha_{\text{bot}} \le \alpha \le \alpha_{\text{top}}$. For each α in this interval, the mean value theorem implies $\phi^{(0)}(\alpha) = \phi^{(0)}(\alpha_{\text{bot}}) + \phi^{(0)}_{\alpha}(\beta)(\alpha - \alpha_{\text{bot}})$ for some β between α and α_{bot}. Therefore, $|\phi^{(0)}(\alpha) - \phi^{(0)}(\alpha_{\text{bot}})| = |\phi^{(0)}_{\alpha}(\beta)(\alpha - \alpha_{\text{bot}})| \le |\phi^{(0)}_{\alpha}(\alpha_{\text{bot}})|(\alpha_{\text{top}} - \alpha_{\text{bot}}) = |\phi^{(0)}(\alpha_{\text{bot}})/\alpha_{\text{bot}}|(\alpha_{\text{top}} - \alpha_{\text{bot}})$. Here we have used the boundary condition (2.5c). We then have

$$\left|\frac{\phi^{(0)}(\alpha) - \phi^{(0)}(\alpha_{\text{bot}})}{\phi^{(0)}(\alpha_{\text{bot}})}\right| \le \frac{\alpha_{\text{top}} - \alpha_{\text{bot}}}{\alpha_{\text{bot}}} \tag{2.7}$$

if $\alpha_{\text{bot}} \le \alpha \le \alpha_{\text{top}}$. The relative change in $\phi^{(0)}$ is thus bounded by the relative change in α. In the ocean, α typically varies by at most 1% or so (Gill [9]), and for that variation of α the eigenfunction $\phi^{(0)}$ is nearly constant.

Suppose that the interval $\alpha_{\text{bot}} \le \alpha \le \alpha_{\text{top}}$ is divided into discrete subintervals, so that the fluid is regarded as a stack of immiscible layers. For the jth mode in the solution, the divergence of the horizontal velocity field is $(\hat{u}^{(j)}_x + \hat{v}^{(j)}_y)\phi^{(j)}(\alpha)$. If $j = 0$, then the divergence is nearly independent of α, so for any (x, y, t) the thicknesses of all layers are changed by approximately the same proportion, and the motion is manifested by variations in the elevation of the free surface at the top of the fluid. On the other hand, when $j \ge 1$ the eigenfunction $\phi^{(j)}$ oscillates and changes sign. Thus, for fixed (x, y, t) some layers are thickened and others are thinned, and the motion is manifested primarily by undulations in surfaces of constant density within the fluid. The mode corresponding to $j = 0$ is the external mode, and the other modes are internal modes.

Now suppose that one wants to split the fast and slow dynamics into separate subproblems for the sake of computational efficiency. The preceding discussion suggests that one might model the fast motions with a two-dimensional system of equations that is independent of depth. In the method of Bleck and Smith [2], the x-component of the external velocity field is approximated by a multiple of $\int_{\alpha_{\text{bot}}}^{\alpha_{\text{top}}} u\, dp = \int_{\alpha_{\text{bot}}}^{\alpha_{\text{top}}} u\, p_\alpha\, d\alpha$. The linearization of this expression is $\int_{\alpha_{\text{bot}}}^{\alpha_{\text{top}}} u\, \tilde{p}_\alpha\, d\alpha$; a comparison with (2.6) shows that if the formula in [2] is applied to the linearized case, then one is computing a projection onto the external mode in which the eigenfunction $\phi^{(0)}$ is approximated by a constant. According to (2.7), this is an accurate approximation, but it is not exact. An alternative is to use an integration with respect to z, which follows the spirit of the Bryan–Cox class of models. In this case one uses a multiple of $\int_{z_{\text{bot}}}^{z_{\text{top}}} u\, dz = \int_{\alpha_{\text{bot}}}^{\alpha_{\text{top}}} u z_\alpha\, d\alpha = \int_{\alpha_{\text{bot}}}^{\alpha_{\text{top}}} u(-\alpha/g)\, p_\alpha\, d\alpha$. The second equality follows from the relation $p_\alpha = -g\alpha^{-1}z_\alpha$, which is equivalent to the hydrostatic condition $p_z = -g\alpha^{-1}$. The linearization of the last integral is $\int_{\alpha_{\text{bot}}}^{\alpha_{\text{top}}} u(-\alpha/g)\, \tilde{p}_\alpha\, d\alpha$; in this case, one is approximating $\phi^{(0)}$ with a linear function of α. This approximation is also inexact.

If an inexact projection is used to split the dynamics into fast and slow subproblems, then the equations that model the slow part of the solution may in fact contain some fast elements. This raises the possibility that if an explicit method is used to solve those equations, then the method could be unstable. In the remainder of this paper we examine the operator splitting of Bleck and Smith and show that linear instabilities can arise in that case.

2.3. *An Operator Splitting*

Here we describe the operator splitting developed by Bleck and Smith [2]. In the following, we use the term ''barotropic'' to refer to the system of equations that approximately models the fast external motions, and we use the term ''baroclinic'' to refer to the system corresponding to the slow internal motions. In the case of linearized dynamics, the external mode is approximately barotropic in the sense of classical fluid dynamics, and it is common practice to refer to this mode as barotropic (Gill [9]). In the present paper, we adopt the convention that the terms ''external'' and ''internal'' refer to the exact modal structure of the linearized primitive equations, and the terms ''barotropic'' and ''baroclinic'' are used in the context of operator splitting to refer to subsystems that approximately describe fast and slow motions, respectively.

We begin with the nonlinear hydrostatic Euler equations (2.1), which can be written in the form

$$\mathbf{u}_t + (\mathbf{u}\cdot\nabla)\mathbf{u} + f\mathbf{k}\times\mathbf{u} = -\nabla M \tag{2.8a}$$

$$M_\alpha = p \tag{2.8b}$$

$$p_{\alpha t} + \nabla\cdot(\mathbf{u}p_\alpha) = 0 \tag{2.8c}$$

where $\mathbf{u}(x, y, \alpha, t) = (u(x, y, \alpha, t), v(x, y, \alpha, t))$. The notation $\mathbf{k}\times\mathbf{u}$ refers to the first two components of the cross product $(0, 0, 1) \times (u, v, 0)$, namely $(-v, u)$.

In [2] the velocity field for fast external motions is approximated by the weighted vertical average

$$\bar{\mathbf{u}}(x, y, t) = \frac{\int_{\alpha_{\text{bot}}}^{\alpha_{\text{top}}} \mathbf{u}(x, y, \alpha, t)\, p_\alpha\, d\alpha}{\int_{\alpha_{\text{bot}}}^{\alpha_{\text{top}}} p_\alpha\, d\alpha} = \frac{1}{p_{\text{bot}}(x, y, t)} \int_{\alpha_{\text{bot}}}^{\alpha_{\text{top}}} \mathbf{u}|\, p_\alpha|\, d\alpha, \tag{2.9a}$$

where $p_{\text{bot}}(x, y, t) = p(x, y, \alpha_{\text{bot}}, t)$, and the pressure at the top of the fluid is assumed to be zero. The relation $p_\alpha = -g\alpha^{-1}z_\alpha$ implies that this vertical average is weighted according to mass. The velocity field $\bar{\mathbf{u}}$ will be regarded as the barotropic velocity field, and the baroclinic velocity field is the quantity $\mathbf{u}'$ defined by

$$\mathbf{u}'(x, y, \alpha, t) = \mathbf{u}(x, y, \alpha, t) - \bar{\mathbf{u}}(x, y, t). \tag{2.9b}$$

This definition implies $\int_{\alpha_{\text{bot}}}^{\alpha_{\text{top}}} \mathbf{u}' p_\alpha\, d\alpha = 0$.

Bleck and Smith split the pressure field by defining

$$p(x, y, \alpha, t) = (1 + \eta(x, y, t))\, p'(x, y, \alpha, t). \quad (2.10)$$

Here, the function p' is intended to represent the pressure field due to static effects and internal motions, and η is a dimensionless quantity that captures the fast external signal. If one assumes $p = p' = 0$ when $\alpha = \alpha_{\text{top}}$, then Eq. (2.10) is equivalent to $p_\alpha = (1 + \eta)\, p'_\alpha$. Equation (2.10) then states that an external signal causes the thickness of each fluid layer to change by the same proportion. This statement is approximately valid, but it is not exact. Typically $|\eta| \ll 1$.

In subsequent calculations it is assumed that $p'(x, y, \alpha_{\text{bot}}, t)$ is independent of t. In the linearized case, free-surface perturbations due to internal motions are small, and undulations of surfaces of constant density within the fluid cause little variation in bottom pressure due to the small density contrasts between layers. There is thus some justification to neglecting time variations in $p'(x, y, \alpha_{\text{bot}}, t)$, and we will denote $p'(x, y, \alpha_{\text{bot}}, t)$ by $p'_{\text{bot}}(x, y)$.

The momentum equation (2.8a) is split as follows. The vertically averaged velocity $\bar{\mathbf{u}}$ is assumed to satisfy the two-dimensional equation

$$\bar{\mathbf{u}}_t + f\mathbf{k} \times \bar{\mathbf{u}} = -\alpha_0 \nabla(p'_{\text{bot}} \eta) + \bar{\mathbf{u}}_t^*; \quad (2.11)$$

this equation is the barotropic momentum equation. This equation can be regarded as a vertical average of the three-dimensional momentum equation (2.8a). The term $-\alpha_0 \nabla(p'_{\text{bot}} \eta)$ can be interpreted as an approximation to the vertical average of $-\nabla M$; the parameter α_0 is supposed to be a representative value of α. The quantity $\bar{\mathbf{u}}_t^*$ serves as an error term in the splitting and includes the vertical average of the nonlinear terms in (2.8a). More precisely, if the error in representing the external dynamics is $\mathbf{q}(x, y, t)$, then $\bar{\mathbf{u}}^*$ is defined by $\bar{\mathbf{u}}^*(x, y, t) = \int_{t_0}^{t} \mathbf{q}(x, y, \tau)\, d\tau$. The baroclinic part of the momentum equation is obtained by subtracting (2.11) from (2.8a) to yield

$$(\mathbf{u}' + \bar{\mathbf{u}}^*)_t + (\mathbf{u} \cdot \nabla)\mathbf{u} + f\mathbf{k} \times \mathbf{u}' = -\nabla M', \quad (2.12a)$$

where

$$M'(x, y, \alpha, t) = M(x, y, \alpha, t) - \alpha_0 p'_{\text{bot}}(x, y)\, \eta(x, y, t). \quad (2.12b)$$

The condition $\int_{\alpha_{\text{bot}}}^{\alpha_{\text{top}}} \mathbf{u}'\, p_\alpha\, d\alpha = 0$ is enforced at each time step; in general, this generates a nonzero increment in the quantity $\bar{\mathbf{u}}^*$, which is then transferred to the barotropic momentum equation (2.11) as a forcing term.

We next consider a splitting of the continuity equation (2.8c). Assume that α_{bot} and α_{top} are independent of (x, y, t), integrate (2.8c) over the interval $\alpha_{\text{bot}} \le \alpha \le \alpha_{\text{top}}$, and use the definition (2.9a) of $\bar{\mathbf{u}}$ to obtain $(\partial p_{\text{bot}}/\partial t) + \nabla \cdot (p_{\text{bot}} \bar{\mathbf{u}}) = 0$. Now insert the splitting $p_{\text{bot}} = (1 + \eta)\, p'_{\text{bot}}$; in the time derivative, use the assumption that $\partial p'/\partial t$ can be neglected when $\alpha = \alpha_{\text{bot}}$, and in the divergence term delete the factor $1 + \eta$, since the magnitude of η is typically small. The result is

$$p'_{\text{bot}} \eta_t + \nabla \cdot (p'_{\text{bot}} \bar{\mathbf{u}}) = 0. \quad (2.13)$$

This will be regarded as the barotropic continuity equation, since it can be used to advance the barotropic variable η with respect to time.

We next need an equation for advancing p' in time, and this will be regarded as a baroclinic continuity equation. Insert the splitting $p = (1 + \eta)\, p'$ into (2.8c) to obtain

$$(1 + \eta)\, p'_{\alpha t} + p'_\alpha \eta_t + \nabla \cdot (\mathbf{u}(1 + \eta)\, p'_\alpha) = 0.$$

Now delete the quantity $1 + \eta$ whenever it appears as a factor, and use the expression for η_t in (2.13) to obtain

$$p'_{\alpha t} + \nabla \cdot (\mathbf{u}'\, p'_\alpha) = -\nabla \cdot (\bar{\mathbf{u}}\, p'_\alpha) + \frac{p'_\alpha}{p'_{\text{bot}}} \nabla \cdot (p'_{\text{bot}} \bar{\mathbf{u}}). \quad (2.14)$$

This completes the derivation of the splitting. The barotropic equations are (2.11) and (2.13), and the baroclinic equations are (2.12) and (2.14).

3. THE CASE OF TWO LAYERS AND ONE HORIZONTAL DIMENSION

We now specialize the splitting described in Section 2.3 to the case of a linearized flow in one horizontal dimension in a fluid with two layers. In the present section, we discretize in the vertical direction, but x and t remain continuous. Discretizations with respect to x and t will be described in Sections 4 and 5 for purposes of stability analysis.

Suppose that the system of Bleck and Smith is linearized about a state where $\eta = 0$, the velocity is zero, and the pressure is given by a function $\tilde{p}(\alpha)$. Also suppose that the bottom of the fluid corresponds to fixed $\alpha = \alpha_{\text{bot}}$, the flow is one-dimensional, and $f = 0$. In the pressure splitting (2.10), let p and p' denote perturbations in the total pressure and baroclinic pressure, respectively. The splitting (2.10) can then be written in the form $\tilde{p}(\alpha) + p = (1 + \eta)(\tilde{p}(\alpha) + p')$. Now neglect the product of η and p', since each is small. The linearization of the splitting (2.10) is then

$$p = p' + \eta \tilde{p}(\alpha). \quad (3.1)$$

A calculation shows that the linearization of the Bleck–Smith system (2.11)–(2.14) is

$$\frac{\partial \overline{u}}{\partial t} = -\alpha_0 \tilde{p}(\alpha_{\text{bot}}) \frac{\partial \eta}{\partial x} + \frac{\partial u^*}{\partial t} \tag{3.2a}$$

$$\frac{\partial \eta}{\partial t} + \frac{\partial \overline{u}}{\partial x} = 0 \tag{3.2b}$$

$$\frac{\partial}{\partial t}(u' + u^*) = -\frac{\partial M'}{\partial x} \tag{3.2c}$$

$$\frac{\partial}{\partial t}\left(\frac{\partial p'}{\partial \alpha}\right) + \left(\frac{\partial \tilde{p}}{\partial \alpha}\right)\frac{\partial u'}{\partial x} = 0 \tag{3.2d}$$

$$\frac{\partial M'}{\partial \alpha} = p = p' + \eta \tilde{p}(\alpha). \tag{3.2e}$$

In the present section we do not denote differentiations by subscripts, as subscripts will be used as part of the notation to describe discretizations. The quantities $\overline{u}$, η, and u^* depend on (x, t), and the quantities u', p', and M' depend on (x, α, t). The quantity M' is defined in terms of the perturbation M in the Montgomery potential by the relation

$$M' = M - \alpha_0 \tilde{p}(\alpha_{\text{bot}})\eta, \tag{3.3}$$

which is a linearization of (2.12b). The first two equations in (3.2) are the barotropic equations, the next two are the baroclinic equations, and the last is a linearization of the hydrostatic relation (2.8b). The boundary conditions at the top and bottom of the fluid are

$$p = p' = 0 \quad \text{if } \alpha = \alpha_{\text{top}} \tag{3.4a}$$

$$M = \alpha p \qquad \text{if } \alpha = \alpha_{\text{bot}}. \tag{3.4b}$$

(See (2.3) and (2.10).) The second condition can be expressed in terms of M' by using (3.3).

3.1. *Vertical Discretization*

Now discretize the above system with respect to the vertical (α) direction. Divide the interval $\alpha_{\text{bot}} \le \alpha \le \alpha_{\text{top}}$ into two subintervals of length $\Delta\alpha$. Fluid flows along surfaces of constant density, in the present model, so this vertical discretization amounts to dividing the fluid into two immiscible layers. In the finite difference formulation that follows, we use centered differences defined relative to a staggered grid. Values of p, p', and $\tilde{p}$ are associated with grid points located on boundaries of layers, and values of u', M', and M are associated with midpoints of layers; see Fig. 3.1. Subscripts are placed on variables to denote the vertical position.

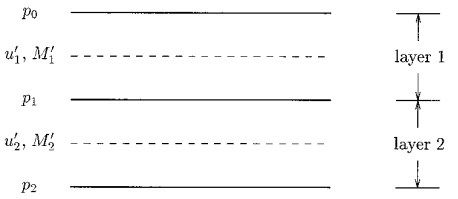

FIG. 3.1. Vertical discretization. In this diagram the horizontal and vertical directions correspond to x and α, respectively. The solid lines indicate boundaries of layers. The locations of the symbols p_0, u_1', M_1', ..., specify the vertical locations of grid points where these quantities are defined.

The baroclinic continuity equation (3.2d) involves derivatives with respect to α. If these derivatives are approximated with second-order centered finite differences, then equation (3.2d) can be approximated by the equation

$$\frac{\partial}{\partial t}(\Delta p_r') + (\Delta \tilde{p}_r)\frac{\partial u_r'}{\partial x} = 0 \tag{3.5}$$

for $r = 1$ and $r = 2$. Here $\Delta p_r' = p_r' - p_{r-1}'$ and $\Delta \tilde{p}_r = \tilde{p}_r - \tilde{p}_{r-1}$; these quantities denote pressure increments across the rth layer. The quantity u_r' is the baroclinic velocity in the rth layer.

As noted in Section 2.3, the condition $\int_{\alpha_{\text{bot}}}^{\alpha_{\text{top}}} \mathbf{u}'\, p_\alpha\, d\alpha = 0$ is enforced at each time step. In the present context, the linearized relation $\int_{\alpha_{\text{bot}}}^{\alpha_{\text{top}}} u'\, d\tilde{p} = 0$ can be approximated by the relation

$$u_1' \Delta \tilde{p}_1 + u_2' \Delta \tilde{p}_2 = 0. \tag{3.6}$$

Now sum Eq. (3.5) over both layers and apply (3.6). The result is that $p_2' = \Delta p_1' + \Delta p_2'$ is independent of time; this is consistent with the assumption made in Section 2.3 that p_{bot}' is independent of t. If $\Delta p_1'$ is known, then $\Delta p_2'$ is determined automatically. Similarly, relation (3.6) implies that u_2' can also be eliminated from the analysis. We will ultimately consider the baroclinic momentum and continuity equations in the top layer only.

The condition (3.2e), $\partial M'/\partial \alpha = p$, can be discretized to yield the interface condition

$$M_1' = M_2' + (\Delta\alpha)p_1 \tag{3.7}$$

between the layers. The bottom boundary condition (3.4b) can be implemented as follows. Values of pressure are defined at grid points lying along the bottom of the lower layer, but values of M and M' are defined at points located in the middle of that layer. Let $\alpha_2 = \alpha_{\text{bot}} + \Delta\alpha/2$; this is

the value of α associated with the middle of the lower layer. A Taylor expansion with respect to α yields

$$M(x, \alpha_2, t) = \alpha_{\text{bot}} p_{\text{bot}} + (\Delta\alpha/2)(\partial M/\partial\alpha) + O(\Delta\alpha)^2$$
$$= (\alpha_{\text{bot}} + \Delta\alpha/2)p_{\text{bot}} + O(\Delta\alpha)^2.$$

The last equality relies on the relation $\partial M/\partial\alpha = p$. (See (3.2e) and (3.3).) The bottom boundary condition (3.4b) can therefore be approximated by $M_2 = \alpha_2 p_{\text{bot}} = \alpha_2 p_2$. The relations (3.1) and (3.3) then yield $M_2' = \alpha_2 p_2' + (\alpha_2 - \alpha_0)\tilde{p}_2\eta$. For the sake of simplicity, we choose $\alpha_0 = \alpha_2$. The bottom boundary condition is then

$$M_2' = \alpha_2 p_2'. \tag{3.8}$$

As observed earlier, p_2' is independent of t, so M_2' is determined by the initial data.

The preceding discussion has been concerned with finite difference approximations in the vertical direction for a continuously stratified fluid. One can also develop these ideas in the context of a discretely stratified fluid consisting of two homogeneous layers having constant specific volumes α_1 and α_2. For example, the hydrostatic assumption implies that the Montgomery potential is independent of depth in a region of constant density; continuity of position and pressure across an interface then implies that the jump condition (3.7) is exact in the discrete case. It can be verified that the other preceding approximations for a continuously stratified fluid are exact conditions for a discretely stratified fluid.

3.2. *Baroclinic System*

In this subsection we formulate in detail the baroclinic equations for a two-layer model. For reasons given earlier, it suffices to consider baroclinic equations for the upper layer only. The baroclinic continuity equation can be taken to be Eq. (3.5) with $r = 1$. We now obtain an explicit form of the momentum equation.

The baroclinic momentum equation (3.2c) for layer r can be written in the form

$$\frac{\partial}{\partial t}(u_r' + u^*) = -\frac{\partial M_r'}{\partial x}. \tag{3.9}$$

Here, $r = 1$ or $r = 2$. The quantity u^* is included in order to make it possible for the vertical mean of u' to be zero at all times; for the case of two layers, this condition is expressed by Eq. (3.6). We now use this property to identify $\partial u^*/\partial t$ and eliminate it from (3.9).

Multiply (3.9) by $\Delta\tilde{p}_r$, sum over r, and use (3.6) and the relation $\tilde{p}_2 = \Delta\tilde{p}_1 + \Delta\tilde{p}_2$ to obtain

$$\tilde{p}_2 \frac{\partial u^*}{\partial t} = -\frac{\partial}{\partial x}(\Delta\tilde{p}_1 M_1' + \Delta\tilde{p}_2 M_2').$$

The interface condition (3.7) then yields

$$\frac{\partial u^*}{\partial t} = -\frac{\partial}{\partial x}\left(M_2' + \frac{\Delta\tilde{p}_1}{\tilde{p}_2} p_1 \Delta\alpha\right). \tag{3.10}$$

Now insert this expression for $\partial u^*/\partial t$ back into the momentum equation (3.9) for $r = 1$ to obtain

$$\frac{\partial u_1'}{\partial t} = -\frac{\Delta\tilde{p}_2}{\tilde{p}_2}(\Delta\alpha)\frac{\partial p_1}{\partial x}. \tag{3.11}$$

The pressure splitting (3.1) and the top boundary condition (3.4a) imply $p_1 = \Delta p_1 = \Delta p_1' + \eta\Delta\tilde{p}_1$. This can be inserted into (3.11) to give an alternate form of the baroclinic momentum equation for the upper layer. When this form is combined with the baroclinic continuity equation (3.5) with $r = 1$, the result is the system

$$\frac{\partial}{\partial t}\begin{pmatrix}\Delta p_1' \\ u_1'\end{pmatrix} + \begin{pmatrix}0 & \Delta\tilde{p}_1 \\ (\Delta\tilde{p}_2)(\Delta\alpha)/\tilde{p}_2 & 0\end{pmatrix}\frac{\partial}{\partial x}\begin{pmatrix}\Delta p_1' \\ u_1'\end{pmatrix} = \begin{pmatrix}0 \\ -(\Delta\tilde{p}_1\,\Delta\tilde{p}_2\,\Delta\alpha/\tilde{p}_2)(\partial\eta/\partial x)\end{pmatrix}. \tag{3.12}$$

The vector on the right side of (3.12) can be regarded as a forcing term.

The wave velocities for the system (3.12) are given by the eigenvalues of the coefficient matrix of the x-derivative. These eigenvalues are $\pm c_1$, where

$$c_1 = \sqrt{(\Delta\tilde{p}_1)(\Delta\tilde{p}_2)(\Delta\alpha)/\tilde{p}_2}. \tag{3.13}$$

This quantity is the speed of internal waves in a fluid with two layers, under the present model. The baroclinic system (3.12) can then be written in the form

$$\frac{\partial}{\partial t}\left(\frac{\Delta p_1'}{\Delta\tilde{p}_1}\right) + c_1\frac{\partial}{\partial x}\left(\frac{u_1'}{c_1}\right) = 0 \tag{3.14a}$$

$$\frac{\partial}{\partial t}\left(\frac{u_1'}{c_1}\right) + c_1\frac{\partial}{\partial x}\left(\frac{\Delta p_1'}{\Delta\tilde{p}_1}\right) = -c_1\frac{\partial\eta}{\partial x}, \tag{3.14b}$$

in which the dependent variables are nondimensional.

3.3. *Barotropic System*

We now describe the barotropic equations (3.2a)–(3.2b) in greater detail, especially in relation to the two-layer

baroclinic system of Section 3.2. The barotropic momentum equation (3.2a) contains a forcing term $\partial u^*/\partial t$. In the formulation used by Bleck and Smith [2], the baroclinic equations (2.12) and (2.14) are solved over the time interval $t_n \le t \le t_{n+1}$ before the barotropic equations are solved over that time interval. The solution of the baroclinic equations yields a time increment $\Delta^{n+1}u^*$ in the quantity u^*, and the forcing term $\partial u^*/\partial t$ is then approximated by the constant $\Delta^{n+1}u^*/\Delta t$ for $t_n \le t \le t_{n+1}$. (Here $\Delta t = t_{n+1} - t_n$). After this approximation is made, the barotropic equations have the form

$$\frac{\partial}{\partial t}\begin{pmatrix}\overline{u}\\ \eta\end{pmatrix} + \begin{pmatrix}0 & \alpha_2\tilde{p}_2\\ 1 & 0\end{pmatrix}\frac{\partial}{\partial x}\begin{pmatrix}\overline{u}\\ \eta\end{pmatrix} = \begin{pmatrix}\Delta^{n+1}u^*/\Delta t\\ 0\end{pmatrix} \quad (3.15)$$

for $t_n \le t \le t_{n+1}$. Here, we use $\tilde{p}(\alpha_{\text{bot}}) = \tilde{p}_2$ and $\alpha_0 = \alpha_2$, as described in Section 3.1.

The system (3.15) has the form of the one-dimensional shallow water equations with a forcing term (Pedlosky [14]). The characteristic velocities are equal to the eigenvalues $\pm c_0$, where

$$c_0 = \sqrt{\alpha_2\tilde{p}_2}. \quad (3.16)$$

This quantity is the speed of external gravity waves, as represented by the model (3.15) of external motions.

A comparison with (3.13) shows that in the case of a fluid with two layers, the internal wave speed c_1 and the external wave speed c_0 are related by

$$\left(\frac{c_1}{c_0}\right)^2 = \left(\frac{\Delta\tilde{p}_1}{\tilde{p}_2}\right)\left(\frac{\Delta\tilde{p}_2}{\tilde{p}_2}\right)\left(\frac{\Delta\alpha}{\alpha_2}\right). \quad (3.17)$$

For example, if $\Delta\tilde{p}_1/\tilde{p}_2 = 0.25$, $\Delta\tilde{p}_2/\tilde{p}_2 = 0.75$, and $\Delta\alpha/\alpha_2 = 0.01$, then $c_1/c_0 \approx 0.043$. Equation (3.17) is an analogue of a relation derived by Gill [9] for a two-layer fluid when the vertical coordinate is z instead of α. The relations (3.13), (3.16), and (3.17) will be used in various nondimensionalizations later.

4. STABILITY ANALYSIS

We next discretize the system (3.14)–(3.15) with respect to x and t and analyze the stability of the resulting algorithm. In the present section the baroclinic system (3.14) is discretized with a forward–backward time stepping scheme and with centered spatial differences on a staggered grid. This discretization is chosen so that the algorithm is stable and nondissipative when the coupling to the barotropic system (3.15) is removed. With this formulation, there is no inherent dissipation to mask any destabilizing effects of the operator splitting, nor is there an underlying instability that could aggravate any such effects of the splitting. Of all the possible discretizations that have this property, the present forward–backward scheme is perhaps the simplest to analyze. Some alternate discretizations are discussed in Section 5.

Our ultimate goal is to perform a von Neumann stability analysis of the algorithm. (See, e.g., Richtmyer and Morton [17].) For this kind of analysis, assume that the system is defined for $-\infty < x < \infty$ and $t > 0$. Apply a Fourier transform with respect to x, and express the transformed solution at time $t_{n+1} = (n+1)\Delta t$ in terms of the transformed solution at time $t_n = n\,\Delta t$. Here, Δt is the time step that is used when solving the slow baroclinic equations. If there exist solutions of the system that are unbounded as the time index tends to infinity, then the algorithm is unstable; otherwise, the algorithm is stable.

In the following discussion, the barotropic system (3.15) is discretized with respect to x but is solved exactly with respect to t over each time interval $t_n \le t \le t_{n+1}$. We use the exact solution with respect to t partly in order to simplify calculations, but mainly so that the analysis cannot be affected by errors arising from a numerical method for integrating the barotropic equations with respect to t; the main issues here are the nature of the splitting and the fact that the baroclinic equations are advanced explicitly with long time steps.

4.1. *Matrix Form of the Algorithm*

In this subsection we discretize the system (3.14)–(3.15) and express the result in matrix–vector form for the sake of later analysis.

In the baroclinic continuity equation (3.14a), we use a forward time difference to express $\Delta p_1'$ at time t_{n+1} in terms of data at time t_n. We then apply a backward time difference to the baroclinic momentum equation (3.14b) to obtain u_1' at time t_{n+1}. For a space discretization, we use centered second-order finite differences on a staggered grid. Values of η and $\Delta p_1'$ are defined at points with spacing Δx, and grid points for $\overline{u}$ and u_1' are located halfway between the points for η and $\Delta p_1'$. The resulting algorithm can be expressed in the form

$$\frac{(\Delta\hat{p}_1')^{n+1}}{\Delta\tilde{p}_1} = \frac{(\Delta\hat{p}_1')^{n}}{\Delta\tilde{p}_1} - (c_1 D)\,\frac{(\hat{u}_1')^{n}}{c_1} \quad (4.1a)$$

$$\frac{(\hat{u}_1')^{n+1}}{c_1} = \frac{(\hat{u}_1')^{n}}{c_1} - (c_1 D)\,\frac{(\Delta\hat{p}_1')^{n+1}}{\Delta\tilde{p}_1} - (c_1 D)\,\hat{\eta}^n. \quad (4.1b)$$

Here $(\Delta\hat{p}_1')^n = (\Delta\hat{p}_1')^n(k)$, $(\hat{u}_1')^n = (\hat{u}_1')^n(k)$, and $\hat{\eta}^n = \hat{\eta}^n(k)$ denote the Fourier transforms of $\Delta p_1'$, u_1', and η with respect to x at time t_n, with k being the dual variable for the

Fourier transform. The action of the spatial differencing is represented by the quantity

$$D = D(k) = \frac{\Delta t}{\Delta x}(e^{ik\Delta x/2} - e^{-ik\Delta x/2}). \tag{4.2}$$

In the formulation of Bleck and Smith [2], the baroclinic equations are updated before the barotropic equations; in the difference scheme (4.1), one would then use η^n, since η^{n+1} is not yet available. An alternative to the time-stepping in (4.1) is to update u_1' first and then update $\Delta p_1'$. In some experiments reported later, this change had no effect on stability. We use the order of updating in (4.1) because in the nonlinear analogue it would be natural to update p' first, since one might want the factors in the divergence term $\nabla \cdot (\mathbf{u} p_\alpha')$ in (2.14) to be evaluated at the same time level.

Next consider the barotropic system (3.15). After a Fourier transform is applied with respect to x, the system can be written in the form

$$\frac{\partial}{\partial t}\begin{pmatrix} \hat{\bar{u}}(k,t)/c_0 \\ \hat{\eta}(k,t) \end{pmatrix} = B\begin{pmatrix} \hat{\bar{u}}/c_0 \\ \hat{\eta} \end{pmatrix} + \begin{pmatrix} \Delta^{n+1}\hat{u}^*/(c_0\Delta t) \\ 0 \end{pmatrix}, \tag{4.3a}$$

where

$$B = \frac{-c_0 D}{\Delta t}\begin{pmatrix} 0 & 1 \\ 1 & 0 \end{pmatrix}, \tag{4.3b}$$

and c_0 is given by (3.16). The eigenvalues of B are $-c_0 D/\Delta t$ and $c_0 D/\Delta t$; corresponding eigenvectors are $(1, 1)^{\mathrm{T}}$ and $(1, -1)^{\mathrm{T}}$, respectively. The solution of (4.3) that satisfies the initial conditions $\hat{\bar{u}}(k, t_n) = \hat{\bar{u}}^n(k)$ and $\hat{\eta}(k, t_n) = \hat{\eta}^n(k)$ is

$$\begin{pmatrix} \hat{\bar{u}}(k,t)/c_0 \\ \hat{\eta}(k,t) \end{pmatrix} = Y(t-t_n)\begin{pmatrix} \hat{\bar{u}}^n(k)/c_0 \\ \hat{\eta}^n(k) \end{pmatrix} + (I - Y(t-t_n))\begin{pmatrix} 0 \\ \Delta^{n+1}\hat{u}^*/(c_0^2 D) \end{pmatrix}, \tag{4.4a}$$

where

$$Y(t-t_n) = V\begin{pmatrix} e^{(-c_0 D/\Delta t)(t-t_n)} & 0 \\ 0 & e^{(c_0 D/\Delta t)(t-t_n)} \end{pmatrix} V^{-1}, \tag{4.4b}$$

with

$$V = \begin{pmatrix} 1 & 1 \\ 1 & -1 \end{pmatrix}. \tag{4.4c}$$

The terms in (4.4a) that involve $Y(t - t_n)$ are solutions of the homogeneous analogue of (4.3). The updated values $\hat{\bar{u}}^{n+1}$ and $\hat{\eta}^{n+1}$ are then obtained by letting $t - t_n = \Delta t$ in (4.4a)–(4.4b). The final result is

$$\begin{pmatrix} \hat{\bar{u}}^{n+1}/c_0 \\ \hat{\eta}^{n+1} \end{pmatrix} = Y(\Delta t)\begin{pmatrix} \hat{\bar{u}}^n/c_0 \\ \hat{\eta}^n \end{pmatrix} + (I - Y(\Delta t))\begin{pmatrix} 0 \\ \Delta^{n+1}\hat{u}^*/(c_0^2 D) \end{pmatrix}, \tag{4.5a}$$

where

$$Y(\Delta t) = V\begin{pmatrix} e^{-c_0 D} & 0 \\ 0 & e^{c_0 D} \end{pmatrix} V^{-1}. \tag{4.5b}$$

We next obtain an explicit representation for the term $\Delta^{n+1}\hat{u}^*/(c_0^2 D)$ in (4.5). A comparison of (3.10) and the linearized pressure splitting (3.1) yields

$$\frac{\partial u^*}{\partial t} = -\left(\frac{\Delta\tilde{p}_1}{\tilde{p}_2}\right)(\Delta\alpha)\frac{\partial}{\partial x}(\Delta p_1' + (\Delta\tilde{p}_1)\eta) - \frac{\partial M_2'}{\partial x}.$$

In the method of Bleck and Smith [2], a time increment in the quantity u^* is obtained by updating the baroclinic momentum equation (2.12) or (3.9) in each layer and then enforcing the requirement that the values of the baroclinic velocity u' have vertical mean zero. In the time stepping described in (4.1), the update of baroclinic velocity involves the quantities $(\Delta\hat{p}_1')^{n+1}$ and $\hat{\eta}^n$, so we use

$$\Delta^{n+1}\hat{u}^* = -\left(\frac{\Delta\tilde{p}_1}{\tilde{p}_2}\right)(\Delta\alpha)D((\Delta\hat{p}_1')^{n+1} + (\Delta\tilde{p}_1)\hat{\eta}^n) - D\hat{M}_2'. \tag{4.6}$$

An alternate derivation is to apply the forward–backward time stepping used in (4.1) to the baroclinic momentum equation (3.9) and baroclinic continuity equation (3.5) in each layer and then impose condition (3.6). A calculation similar to the derivation of (3.10) then yields Eq. (4.6). A comparison with the velocity relations (3.16)–(3.17) produces

$$\frac{\Delta^{n+1}\hat{u}^*}{(c_0^2 D)} = -\left(\frac{\Delta\tilde{p}_1}{\Delta\tilde{p}_2}\right)\left(\frac{c_1}{c_0}\right)^2\left[\frac{(\Delta\hat{p}_1')^{n+1}}{\Delta\tilde{p}_1} + \hat{\eta}^n\right] - \left(\frac{\hat{M}_2'}{c_0^2}\right). \tag{4.7}$$

The last term on the right side is independent of n.

We now combine the discrete equations (4.1), (4.5), and (4.7) into a single vector equation. Let

$$v^n(k) = \left(\frac{(\Delta \hat{p}_1')^n}{\Delta \tilde{p}_1} \quad \frac{(\hat{u}_1')^n}{c_1} \quad \frac{\hat{\bar{u}}^n}{c_0} \quad \hat{\eta}^n \right)^{\mathrm{T}} \tag{4.8a}$$

denote a column vector of unknowns, and let

$$Z(\Delta t) = \left(\frac{\Delta \tilde{p}_1}{\Delta \tilde{p}_2} \right) \left(\frac{c_1}{c_0} \right)^2 (I - Y(\Delta t)). \tag{4.8b}$$

Equations (4.1), (4.5), and (4.7) can then be written in the form

$$E_1 v^{n+1} = E_0 v^n + F(k), \tag{4.9a}$$

where

$$E_1 = \begin{pmatrix} 1 & 0 & 0 & 0 \\ c_1 D & 1 & 0 & 0 \\ Z_{12} & 0 & 1 & 0 \\ Z_{22} & 0 & 0 & 1 \end{pmatrix},$$

$$E_0 = \begin{pmatrix} 1 & -c_1 D & 0 & 0 \\ 0 & 1 & 0 & -c_1 D \\ 0 & 0 & Y_{11} & Y_{12} - Z_{12} \\ 0 & 0 & Y_{21} & Y_{22} - Z_{22} \end{pmatrix}, \tag{4.9b}$$

and $F(k)$ is a forcing term that involves initial data and is independent of n.

4.2. *Analysis of the Purely Baroclinic System*

We now show that if the preceding algorithm is restricted to the equations that are intended to model the slow motions, without any forcing from the rest of the system, then the algorithm is stable and nondissipative, provided that the Courant–Friedrichs–Lewy condition $c_1 \, \Delta t/\Delta x < 1$ is satisfied. However, in Section 4.3 we show that the method is unstable when both barotropic and baroclinic motions are present. This instability is apparently due to the inexactness of the operator splitting used here.

We examine the case of slow motions as follows. In the baroclinic equations (4.1), suppose that the forcing term η is identically zero, and let

$$w^n(k) = \begin{pmatrix} (\Delta \hat{p}_1')^n / \Delta \tilde{p}_1 \\ (\hat{u}_1')^n / c_1 \end{pmatrix}.$$

In this case, the algorithm has the form

$$B_1 w^{n+1} = B_0 w^n, \tag{4.10a}$$

where

$$B_1 = \begin{pmatrix} 1 & 0 \\ c_1 D & 1 \end{pmatrix}, \quad B_0 = \begin{pmatrix} 1 & -c_1 D \\ 0 & 1 \end{pmatrix}. \tag{4.10b}$$

The matrices B_1 and B_0 depend on the wavenumber k, since D depends on k (cf. (4.2)). If there exists a k that yields a solution of (4.10) that is unbounded as n increases, then the algorithm is unstable, in the von Neumann sense; otherwise, the algorithm is stable (Richtmyer and Morton [17]).

PROPOSITION 4.1. *The algorithm* (4.10) *is stable if* $c_1 \, \Delta t/\Delta x < 1$.

Proof. We begin by seeking solutions of the form $w^n = \lambda^n q$, where λ is a complex scalar and q is a nonzero vector. The superscript on λ is an exponent, and the superscript on w is a time index. A form $w^n = \lambda^n q$ satisfies the difference equation (4.10) if and only if $\lambda B_1 q = B_0 q$. This condition, together with the constraint $q \neq 0$, will be regarded as an eigenvalue problem with eigenvalue λ. A number λ is an eigenvalue if and only if $\det(\lambda B_1 - B_0) = 0$, or

$$\lambda^2 - a\lambda + 1 = 0, \tag{4.11a}$$

where

$$a = 2 + c_1^2 D^2 = 2 + \left(\frac{c_1 \, \Delta t}{\Delta x} \right)^2 (e^{ik\Delta x} - 2 + e^{-ik\Delta x}). \tag{4.11b}$$

If $c_1 \, \Delta t/\Delta x < 1$, then $-2 < a \leq 2$. If $-2 < a < 2$, then the roots of (4.11a) have nonzero imaginary parts; since a is real, the roots are complex conjugates. Denote these roots by λ_1 and $\lambda_2 = \overline{\lambda_1}$. In (4.11a), the coefficient of λ^2 is 1, so the product of the roots is equal to the constant term. Thus $1 = \lambda_1 \lambda_2 = \lambda_1 \overline{\lambda_1} = |\lambda_1|^2 = |\lambda_2|^2$. The eigenvalues λ_1 and λ_2 are distinct, so corresponding eigenvectors q_1 and q_2 must be linearly independent. It then follows that every solution of (4.10) can be written as a linear combination of $\lambda_1^n q_1$ and $\lambda_2^n q_2$. Since $|\lambda_1| = |\lambda_2| = 1$, each of these solutions is bounded as n increases. In the remaining case $a = 2$, a comparison with (4.11b) shows that $D = 0$; it then follows from (4.10) that $w^{n+1} = w^n$ for all n. Therefore, for each k, all solutions of the difference equation (4.10) are bounded, and the algorithm is stable. This completes the proof.

Since $|\lambda_1| = |\lambda_2| = 1$ when $-2 < a < 2$, each of the

terms $\lambda_1^n q_1$ and $\lambda_2^n q_2$ maintains a constant amplitude as n increases. In this sense, the algorithm (4.10) is nondissipative.

4.3. *Analysis of the Coupled Barotropic–Baroclinic System*

We now examine the general algorithm (4.9). In the following proof of instability, it suffices to examine the corresponding homogeneous system $E_1 v^{n+1} = E_0 v^n$. The matrices E_1 and E_0 depend on k, since D depends on k. If there exists k for which the homogeneous system $E_1 v^{n+1} = E_0 v^n$ has solutions that are unbounded as n increases, then the algorithm is unstable.

Again, we begin by seeking solutions of the form $v^n = \lambda^n q$, where now q is a vector having four components. This form is a nontrivial solution of the homogeneous system if and only if λ and q satisfy the eigenvalue problem

$$\lambda E_1 q = E_0 q, \quad q \neq 0. \tag{4.12}$$

A number λ is an eigenvalue if and only if $\det(\lambda E_1 - E_0) = 0$. A calculation shows that this condition is equivalent to

$$(\lambda^2 - a\lambda + 1)(\lambda^2 - b\lambda + 1) + \delta(k)(\lambda + 1)(\lambda - 1)^2 = 0, \tag{4.13a}$$

where a is defined in (4.11b), $b = \exp(-c_0 D) + \exp(c_0 D)$, and

$$\begin{aligned}\delta(k) &= \left(\frac{\Delta\tilde{p}_1}{\Delta\tilde{p}_2}\right)\left(\frac{c_1}{c_0}\right)^2\left[1 - \frac{1}{2}(e^{-c_0 D} + e^{c_0 D})\right] \\ &= \left(\frac{\Delta\alpha}{\alpha_2}\right)\left(\frac{\Delta\tilde{p}_1}{\tilde{p}_2}\right)^2\left[1 - \cos\left(2\frac{c_0\,\Delta t}{\Delta x}\sin(k\,\Delta x/2)\right)\right] \\ &\equiv \left(\frac{\Delta\alpha}{\alpha_2}\right) S(k). \end{aligned} \tag{4.13b}$$

Equations (4.13a)–(4.13b) were obtained with the aid of the computer algebra systems Maple V and Mathematica. During independent calculations, the two systems yielded the same results. The relations in (4.13b) rely on Eqs. (3.17) and (4.2), and the last equality in (4.13b) contains the definition of an oscillatory function $S(k)$.

The characteristic polynomial on the left side of (4.13a) will be regarded as a small perturbation of the simpler polynomial $(\lambda^2 - a\lambda + 1)(\lambda^2 - b\lambda + 1)$, since the factor $\Delta\alpha/\alpha_2$ in $\delta(k)$ is typically small. The factor $S(k)$ in $\delta(k)$ is always nonnegative and oscillates between a minimum of 0 and a maximum of $2(\Delta\tilde{p}_1/\tilde{p}_2)^2$. Due to periodicity, the problem (4.13) can be restricted to the interval $-\pi < k\,\Delta x \leq \pi$.

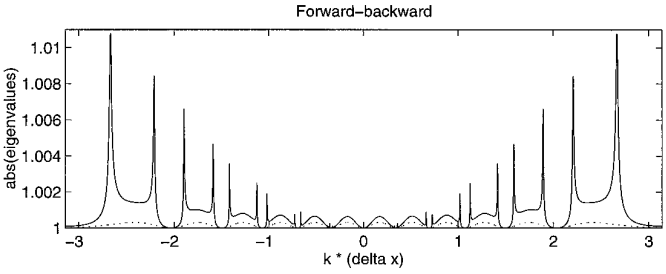

FIG. 4.1. Plots of eigenvalues versus wavenumber. Here we consider a two-layer model for which $\Delta\tilde{p}_1/\tilde{p}_2 = 0.25$, $\Delta\tilde{p}_2/\tilde{p}_2 = 0.75$, $\Delta\alpha/\alpha_2 = 0.01$, and $c_1\,\Delta t/\Delta x = 0.8$. The solid curve shows the maximum of the absolute values of the eigenvalues of the problem (4.12) corresponding to the algorithm (4.9). The maximum moduli are plotted as a function of the dimensionless wavenumber $k\,\Delta x$. The dotted curve is a graph of the lower bound in (4.14). Instability follows from the fact that there exist eigenvalues having modulus greater than 1.

PROPOSITION 4.2. *The algorithm* (4.9) *is unstable, for any value of the Courant number* $c_1\,\Delta t/\Delta x$. *Furthermore, for each* k *let* $\max|\lambda(k)|$ *denote the maximum of the absolute values of the eigenvalues of* (4.12). *Then*

$$\begin{aligned}\max|\lambda(k)| &\geq (1 + \delta(k))^{1/4} = 1 \\ &\quad + \frac{1}{4}\left(\frac{\Delta\alpha}{\alpha_2}\right) S(k) + O\left(\frac{\Delta\alpha}{\alpha_2}\right)^2 \end{aligned} \tag{4.14}$$

for all k.

Proof. In the characteristic polynomial on the left side of (4.13a), the coefficient of λ^4 is 1, so the product of the eigenvalues is equal to the constant term $1 + \delta(k)$. If the eigenvalues are denoted by λ_i for $1 \leq i \leq 4$, then $(\max|\lambda(k)|)^4 \geq |\lambda_1\lambda_2\lambda_3\lambda_4| = 1 + \delta(k)$. Thus $\max|\lambda(k)| \geq (1 + \delta(k))^{1/4} = 1 + \delta(k)/4 + O(\delta(k))^2$. The relation (4.14) is thus established. The quantity $(1 + \delta(k))^{1/4}$ is strictly greater than 1 for almost all k; for any such k there therefore exists an eigenvalue λ such that $|\lambda| > 1$. This implies that there exist solutions of the homogeneous system that have the form $\lambda^n q$ with $|\lambda| > 1$ and $q \neq 0$. Such solutions grow exponentially as functions of the time index n, so the algorithm (4.9) is unstable. This completes the proof.

An example of the behavior of the eigenvalues is illustrated in Fig. 4.1. In this example, we consider a two-layer model for which $\Delta\tilde{p}_1/\tilde{p}_2 = 0.25$, $\Delta\tilde{p}_2/\tilde{p}_2 = 0.75$, and $\Delta\alpha/\alpha_2 = 0.01$; and we assume that Δt and Δx are chosen so that the Courant number is $c_1\,\Delta t/\Delta x = 0.8$. We considered values of $k\,\Delta x$ varying from $-\pi$ to π in increments of $\pi/1600$, and for each such $k\,\Delta x$ we computed the maximum of the absolute values of the eigenvalues of (4.12). We then plotted these maximum moduli as functions of $k\,\Delta x$. The instability of the algorithm is evident from the figure.

The eigenvalues were computed and plotted with the numerical software package Matlab.

The dotted curve in Fig. 4.1 is a plot of the lower bound given on the right side of the inequality in (4.14). This lower bound is considerably less than the actual absolute values of the eigenvalues in some cases, and it appears to have about half the amplitude of the oscillations of the actual eigenvalues near $k = 0$. The discrepancy near $k = 0$ can be explained as follows. Suppose that two of the eigenvalues have absolute values less than or equal to 1; this is the case in the present example, and it has been the case in numerous other examples that we tested. Denote these eigenvalues by λ_3 and λ_4. The proof of inequality (4.14) can then be modified to yield $(\max|\lambda(k)|)^2 \geq |\lambda_1\lambda_2| \geq |\lambda_1\lambda_2\lambda_3\lambda_4| = 1 + \delta(k)$, so $\max|\lambda(k)| \geq (1 + \delta(k))^{1/2} = 1 + \delta(k)/2 + O(k))^2$. In practice, the quantity $(1 + \delta(k))^{1/2}$ may be a valid lower bound for the growth rate.

The preceding discussion implies that $\max|\lambda(k)|$ is bounded below by a rapidly oscillating function of k. In particular, as $|k\ \Delta x|$ varies from zero, $\max|\lambda(k)|$ must move quickly from 1 to values that are greater than 1. The first maximum of the lower bound occurs when $2(c_0\ \Delta t/\Delta x)\sin(k\ \Delta x/2) = \pi$, or $\sin(k\ \Delta x/2) = (\pi/2\nu))(c_1/c_0) = O(\sqrt{\Delta\alpha/\alpha_2})$, where $\nu = c_1\ \Delta t/\Delta x$ (cf. (3.17)). Since $k = 2\pi/L$, where L is wavelength, we then have the first maximum arising for waves that satisfy $\Delta x/L = O(\sqrt{\Delta\alpha/\alpha_2})$. Such waves are long relative to Δx and thus are resolved well by the grid; for example, with the parameters used in Fig. 4.1, the first maximum corresponds to approximately 37 grid intervals per wavelength. If one wishes to stabilize this algorithm via dissipation and/or filtering processes, then apparently these processes must be designed to have significant action on waves that are resolved well by the grid, not just on the very short waves that are typically regarded as numerical artifacts. But the well-resolved waves would presumably be part of the dynamics that one is trying to model. Dissipation and/or filtering would thus amount to overriding the solution of the partial differential equations in a manner that is not necessarily based on model physics.

In the discretization of the baroclinic equations in (4.1), the continuity equation was used to update $\Delta\hat{p}_1'$, and then the momentum equation was used to update u_1'. Some additional experiments were performed in which the baroclinic equations were updated in reverse order. For various choices of parameters, the plots of absolute values of eigenvalues versus wavenumber were essentially the same as those obtained with the time stepping in (4.1).

One source of the instability discussed in this section may be the vertical average that is used to obtain the barotropic velocity $\overline{u}$. This average assumes, in effect, that the external motions are independent of depth; this is a good approximation but is not exact, as discussed in Section 2.2. The pressure splitting (2.10) also assumes that the external motions are independent of depth. Another source of inexactness in the splitting is the gradient term $-\alpha_0\nabla(p_{\text{bot}}'\eta)$ in the barotropic momentum equation (2.11); in effect, this represents an approximation to the vertical average of the term $-\nabla M$ in the three-dimensional momentum equation (2.8a).

4.4. *Discussion of the Perturbations of Roots*

The lower bound in (4.14) does not explain the relatively large values of $|\lambda|$ seen near the ends of the interval $|k\ \Delta x| \leq \pi$. We now sketch how it is possible for eigenvalues to have magnitude $1 + O(\sqrt{\delta(k)})$, not just $1 + O(\delta(k))$. The characteristic polynomial on the left side of (4.13a) is a perturbation of the polynomial

$$r(\lambda) = (\lambda^2 - a\lambda + 1)(\lambda^2 - b\lambda + 1).$$

We begin by examining the roots of r and then consider the effects of the perturbation.

If $c_1\ \Delta t/\Delta x < 1$, then $-2 < a \leq 2$, as observed in the proof of Proposition 4.1. The roots of the factor $(\lambda^2 - a\lambda + 1)$ thus lie on the unit circle. The factor $(\lambda^2 - a\lambda + 1)$ is the characteristic polynomial for the purely baroclinic equations (see (4.11a)), so these roots are associated with baroclinic motions. As $|k\ \Delta x|$ varies from 0 to π with $c_1\ \Delta t/\Delta x$ fixed, the parameter a varies from 2 to $2 - 4(c_1\ \Delta t/\Delta x)^2$, so the roots move in opposite directions around the unit circle from 1 toward -1.

The parameter b in (4.13a) satisfies $|b| \leq 2$ for all k and for all values of $c_1\ \Delta t/\Delta x$. The roots of the factor $(\lambda^2 - b\lambda + 1)$ thus lie on the unit circle. The parameter b can be written in the form

$$b = 2\cos\left(2\left(\frac{c_0}{c_1}\right)\left(\frac{c_1\,\Delta t}{\Delta x}\right)\sin(k\ \Delta x/2)\right).$$

If $c_0/c_1 \gg 1$, as is typical, then the value of b oscillates rapidly as $|k\ \Delta x|$ varies from 0 to π, and the corresponding roots of $(\lambda^2 - b\lambda + 1)$ move around the unit circle several times. If such a root is written in the form $\lambda = \exp(i\omega\ \Delta t)$, then the time dependence in the corresponding mode in the solution of the partial differential equations is $\lambda^n = \exp(i\omega t_n)$. The argument of λ is thus proportional to frequency, and the rapid movement of the root implies that ω is a rapidly changing function of k. This implies large wave velocities, so the roots of $(\lambda^2 - b\lambda + 1)$ can be associated with barotropic motions.

The roots of the polynomial r can thus be divided into two pairs. One pair moves slowly around a portion of the unit circle as $k\ \Delta x$ is varied, and the other pair moves around the circle repeatedly. We will regard these roots as baroclinic roots and barotropic roots, respectively. For

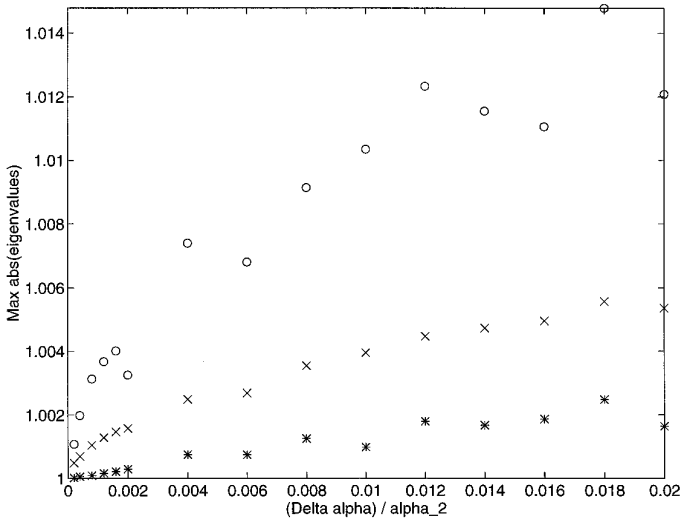

FIG. 4.2. Growth rates as a function of $\Delta\alpha/\alpha_2$. Here we assume $\Delta\tilde{p}_1/\tilde{p}_2 = 0.25$, $\Delta\tilde{p}_2/\tilde{p}_2 = 0.75$, and $c_1\,\Delta t/\Delta x = 0.8$. Each point illustrates the maximum of the absolute values of the eigenvalues over all $k\,\Delta x$, for some numerical method and some value of $\Delta\alpha/\alpha_2$. Circles correspond to the algorithm (4.9), which is based on a forward–backward time stepping for the baroclinic equations. The crosses and asterisks correspond to two predictor–corrector schemes described in Section 5.2.

certain values of $k\,\Delta x$ and the other parameters, the two pairs of roots coincide, and the characteristic polynomial on left side of (4.13a) is thus a perturbation of a polynomial having two double roots. Otherwise, the characteristic polynomial is a perturbation of a polynomial having four distinct roots. If r happens to have distinct roots, then a calculation shows that the roots are perturbed by an amount having magnitude $O(\delta)$. However, in the case of double roots, the perturbation has magnitude $O(\sqrt{\delta})$. The absolute value of the perturbed root is also influenced by the direction of the perturbation. A geometrical argument based on the law of cosines shows that if the magnitude of the perturbation is $O(\sqrt{\delta})$ and if the direction of the perturbation happens to be tangent to the unit circle, then the absolute value of the perturbed root is $1 + O(\delta)$; otherwise, the perturbed root has magnitude $1 + O(\sqrt{\delta})$.

This kind of perturbation is illustrated by an example that is graphed in Fig. 4.2. Consider a two-layer model for which $\Delta\tilde{p}_1/\tilde{p}_2 = 0.25$ and $\Delta\tilde{p}_2/\tilde{p}_2 = 0.75$, and suppose that the Courant number is fixed to have the value $c_1\,\Delta t/\Delta x = 0.8$. For various values of the density contrast $\Delta\alpha/\alpha_2$ between the two layers, we computed eigenvalues of (4.12) for values of $k\,\Delta x$ varying from $-\pi$ to π in increments of $\pi/400$. For each value of $\Delta\alpha/\alpha_2$, we then determined the maximum absolute value, over all k, of the eigenvalues that were computed for that $\Delta\alpha/\alpha_2$. The results can be regarded as measures of the maximum possible growth rates for the various values of $\Delta\alpha/\alpha_2$. The results are graphed with the circles in Fig. 4.2. (The crosses and asterisks represent results from two predictor–corrector algorithms that are discussed in Section 5.2). In this plot, the horizontal axis represents values of $\Delta\alpha/\alpha_2$, and the vertical axis corresponds to the maximum absolute values of eigenvalues. It was shown above that the maximum absolute value of the eigenvalues for fixed k could be as large as $1 + O(\sqrt{\delta(k)})$. If one then computes the maximum absolute value of eigenvalues over all k, it is then possible to have a maximum of $1 + O(\sqrt{\Delta\alpha/\alpha_2})$. The pattern of circles in Fig. 4.2 suggests that this square root dependence may actually occur in the example considered here.

The baroclinic and barotropic roots coincide when the values of the parameters a and b in (4.13a) coincide. A plot of a and b as functions of $k\,\Delta x$ (not shown here) reveals that the values of $k\,\Delta x$ for which $a = b$ are precisely those values corresponding to the sharp spikes in Fig. 4.1. This is to be expected, according to the preceding discussion.

When the barotropic and baroclinic roots coincide, the barotropic and baroclinic modes have the same time dependence, when viewed on the coarse time grid that is used to solve the baroclinic equations. However, the barotropic motions generally oscillate more rapidly than do the baroclinic motions, so the present phenomenon is an example of aliasing. When this aliasing occurs, the effect of the inexactness of the operator splitting is exaggerated, as can be seen from the spikes in Fig. 4.1. This can be regarded as a kind of resonance; it is not a resonance in the physical system, but rather a resonance in the numerical algorithm.

5. ALTERNATE TIME DISCRETIZATIONS

The preceding section was concerned with the stability of the one-dimensional split system (3.14)–(3.15) when a forward–backward time stepping scheme is applied to the baroclinic equations. We now discuss the stability of a leapfrog method and two different predictor–corrector methods. Each algorithm is found to be unstable, so the stability problem is not caused by a peculiarity of one particular time stepping scheme.

5.1. *Leapfrog*

Here we apply a leapfrog time stepping scheme to the baroclinic system (3.14). For a spatial discretization, we use centered second-order finite differences on a staggered grid. Values of η and $\Delta p_1'$ are defined at points with spacing $2\,\Delta x$, and grid points for $\overline{u}$ and u_1' are located halfway between the points for η and $\Delta p_1'$. This is the same spatial discretization as in Section 4, except that a different definition of Δx is used for notational convenience. The formulas that follow are also valid for an unstaggered grid with spacing Δx.

The leapfrog approximation to the baroclinic system (3.14) can be written in the form

$$\frac{(\Delta\hat{p}_1')^{n+1}}{\Delta\tilde{p}_1} = \frac{(\Delta\hat{p}_1')^{n-1}}{\Delta\tilde{p}_1} - (c_1 D_{\mathrm{LF}})\frac{(\hat{u}_1')^n}{c_1}$$

$$\frac{(\hat{u}_1')^{n+1}}{c_1} = \frac{(\hat{u}_1')^{n-1}}{c_1} - (c_1 D_{\mathrm{LF}})\frac{(\Delta\hat{p}_1')^n}{\Delta\tilde{p}_1} - (c_1 D_{\mathrm{LF}})\hat{\eta}^n,$$

where

$$D_{\mathrm{LF}} = D_{\mathrm{LF}}(k) = \frac{\Delta t}{\Delta x}(e^{ik\Delta x} - e^{-ik\Delta x})$$

denotes the action of the spatial differencing in the present case. As in Section 4, we state the algorithm in terms of Fourier transforms with respect to x. We again assume that the barotropic equations are solved exactly with respect to t on the time interval $t_n \le t \le t_{n+1}$.

The barotropic momentum equation (3.2a) contains a forcing term $\partial u^*/\partial t$ that needs to be approximated in the present setting. If a leapfrog method is applied to the baroclinic momentum equation (3.9) in each layer, then a calculation similar to the derivation of (3.10) and (4.6) yields

$$\Delta_{\mathrm{LF}}^{n+1}\hat{u}^* = -\left(\frac{\Delta\tilde{p}_1}{\tilde{p}_2}\right)(\Delta\alpha)D_{\mathrm{LF}}((\Delta\hat{p}_1')^n + (\Delta\tilde{p}_1)\hat{\eta}^n) - D_{\mathrm{LF}}\hat{M}_2'.$$

Here, the quantity $\Delta_{\mathrm{LF}}^{n+1}\hat{u}^*$ represents an increment in u^* between times t_{n-1} and t_{n+1}. The forcing term $\partial u^*/\partial t$ in the barotropic momentum equation (3.2a) can then be approximated by $\Delta_{\mathrm{LF}}^{n+1}\hat{u}^*/(2\,\Delta t)$.

The solution (4.4)–(4.5) of the barotropic system can be applied to the present situation, provided that minor changes are made. First, the quantity $\Delta^{n+1}\hat{u}^*/(c_0^2 D)$ must be replaced by the quantity $\Delta_{\mathrm{LF}}^{n+1}\hat{u}^*/(2c_0^2 D_{\mathrm{LF}})$. A calculation similar to the derivation of (4.7) yields

$$\frac{\Delta_{\mathrm{LF}}^{n+1}\hat{u}^*}{(2c_0^2 D_{\mathrm{LF}})} = -\frac{1}{2}\left(\frac{\Delta\tilde{p}_1}{\Delta\tilde{p}_2}\right)\left(\frac{c_1}{c_0}\right)^2\left[\frac{(\Delta\hat{p}_1')^n}{\Delta\tilde{p}_1} + \hat{\eta}^n\right] - \left(\frac{\hat{M}_2'}{2c_0^2}\right).$$

Second, the quantity $c_0 D/\Delta t$ must be replaced by $c_0 D_{\mathrm{LF}}/2\,\Delta t$ in Eq. (4.3b) and in the definition of $Y(t - t_n)$ in (4.4b).

With these changes in place, let $v^n(k)$ and $Z(\Delta t)$ denote the quantities defined in (4.8). The present algorithm can then be written in the form

$$v^{n+1} = L_0 v^n + L_{-1}v^{n-1} + F(k), \tag{5.1}$$

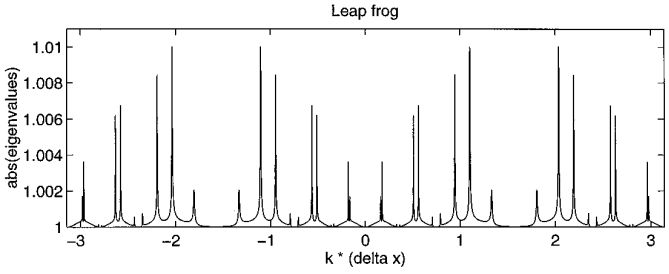

FIG. 5.1. Plots of eigenvalues versus wavenumber, when the baroclinic equations are solved with a leapfrog method. Parameters and axes are the same as in Fig. 4.1.

where

$$L_0 = \begin{pmatrix} 0 & -c_1 D_{\mathrm{LF}} & 0 & 0 \\ -c_1 D_{\mathrm{LF}} & 0 & 0 & -c_1 D_{\mathrm{LF}} \\ -0.5 Z_{12} & 0 & Y_{11} & Y_{12} - 0.5 Z_{12} \\ -0.5 Z_{22} & 0 & Y_{21} & Y_{22} - 0.5 Z_{22} \end{pmatrix},$$

L_{-1} is a diagonal matrix with diagonal entries (1, 1, 0, 0), and $F(k)$ is a forcing term that is independent of n. For purposes of eigenvalue analysis, equation (5.1) can be written in single-step form as

$$\begin{aligned} \begin{pmatrix} v^{n+1} \\ v^n \end{pmatrix} &= \begin{pmatrix} L_0 & L_{-1} \\ I & 0 \end{pmatrix}\begin{pmatrix} v^n \\ v^{n-1} \end{pmatrix} + \begin{pmatrix} F(k) \\ 0 \end{pmatrix} \\ &\equiv G\begin{pmatrix} v^n \\ v^{n-1} \end{pmatrix} + \begin{pmatrix} F(k) \\ 0 \end{pmatrix}. \end{aligned} \tag{5.2}$$

The last equality contains the definition of an 8×8 matrix G. The matrices L_0 and G depend on k, since D_{LF} depends on k.

The stability of the algorithm is governed by the behavior of the homogeneous system $w^{n+1} = Gw^n$, where w^n is a vector having eight components. The problem then reduces to studying the eigenvalue problem $\lambda q = Gq$. The characteristic polynomial has degree 8 in this case, whereas the analysis in Section 4 involves a polynomial of degree 4. The difference is due ultimately to the fact that the leapfrog method uses three time levels, whereas the forward—backward scheme uses two time levels. Due to the greater complexity of the present case, we do not give an analysis here; instead, we restrict the discussion to some numerical computations of eigenvalues.

Figure 5.1 shows a plot having the same format as Fig. 4.1. In this example, we assume $\Delta\tilde{p}_1/\tilde{p}_2 = 0.25$, $\Delta\tilde{p}_2/\tilde{p}_2 =$

0.75, $\Delta\alpha/\alpha_2 = 0.01$, and $c_1\,\Delta t/\Delta x = 0.8$. The vertical coordinate is the maximum absolute value of the eigenvalues of the matrix G in (5.2), and the horizontal coordinate represents values of $k\,\Delta x$ varying from $-\pi$ to π in increments of $\pi/1600$. Plots for a few other values of $\Delta\alpha/\alpha_2$ showed similar behavior. Throughout most portions of the interval $-\pi \le k\,\Delta x \le \pi$, the maximum modulus of the eigenvalues is greater than 1, so the algorithm is unstable. A comparison with Fig. 4.1 suggests that the average of $\max|\lambda|$ over all k is slightly less for the leapfrog scheme than for the forward–backward scheme.

5.2. *Predictor–Corrector Methods*

Here we use the forward–backward algorithm developed in Section 4.1 to obtain an initial estimate of the solution at time t_{n+1}, and we then insert the predicted values into an implicit method for the baroclinic equations to obtain revised values of $\Delta p_1'$ and u_1'. We consider two variations on this theme which use different representations of the barotropic forcing on the baroclinic equations.

Let

$$v^{\text{pred}}(k) = \left(\frac{(\Delta\hat{p}_1')^{\text{pred}}}{\Delta\tilde{p}_1} \; \frac{(\hat{u}_1')^{\text{pred}}}{c_1} \; \frac{\hat{\bar{u}}^{\text{pred}}}{c_0} \; \hat{\eta}^{\text{pred}} \right)^{\mathrm{T}} \tag{5.3}$$

denote a column vector of predicted values of the dependent variables. The prediction step is then

$$E_1 v^{\text{pred}} = E_0 v^n + F(k), \tag{5.4}$$

where E_1, E_0, and $F(k)$ are defined in (4.9). In this step, $\Delta p_1'$ is predicted first, and the result is then used when predicting the baroclinic velocity u_1'.

During the correction step, we will use centered differencing with respect to t, together with a time-averaging of dependent variables. We first correct the velocity u_1' and then correct $\Delta p_1'$. Some experiments with the reverse ordering yielded unstable methods; the computed eigenvalues were far larger than the eigenvalues associated with the predictor step alone. The equations that we will use for the corrector step are

$$\frac{(\Delta\hat{p}_1')^{n+1}}{\Delta\tilde{p}_1} = \frac{(\Delta\hat{p}_1')^{n}}{\Delta\tilde{p}_1} - \frac{c_1 D}{2}\left(\frac{(\hat{u}_1')^{n+1}}{c_1} + \frac{(\hat{u}_1')^{n}}{c_1} \right) \tag{5.5a}$$

$$\frac{(\hat{u}_1')^{n+1}}{c_1} = \frac{(\hat{u}_1')^{n}}{c_1} - \frac{c_1 D}{2}\left(\frac{(\Delta\hat{p}_1')^{\text{pred}}}{\Delta\tilde{p}_1} + \frac{(\Delta\hat{p}_1')^{n}}{\Delta\tilde{p}_1} \right) - (c_1 D)\,\hat{\eta}_{\text{ave}} \tag{5.5b}$$

(cf. (4.1)). The second equation would be implemented first; the equations are written in this order so as to be consistent with the ordering of unknowns in the vectors in (4.8a) and (5.3). In the following, we do not apply a correction step to the barotropic equations, so $\bar{u}^{n+1} = \bar{u}^{\text{pred}}$ and $\eta^{n+1} = \eta^{\text{pred}}$.

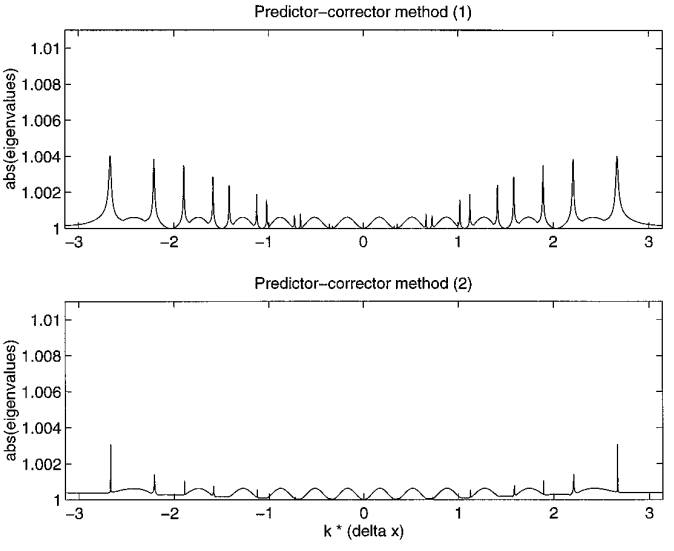

FIG. 5.2. Plots of eigenvalues versus wavenumber, when predictor–corrector methods are used to solve the baroclinic equations.

In Eq. (5.5b), the quantity η_{ave} represents a time average of values of η. Here we consider two possibilities for this average:

(1) Use $\eta_{\text{ave}} = (\eta^{\text{pred}} + \eta^n)/2$.

(2) In the formulation of Bleck and Smith [2], the barotropic equations are solved using many small substeps of the time interval $t_n \le t \le t_{n+1}$; η_{ave} can then be the average of the values of η that are computed over all of those substeps. In the present analysis, we have solved the barotropic equations exactly with respect to t in order to isolate the effects of the operator splitting and baroclinic time stepping. In the analysis that follows, we will simulate the above averaging by using averages of the exact solution over J substeps of the interval $t_n \le t \le t_{n+1}$, where J is the smallest integer that is greater than or equal to c_0/c_1.

For each averaging scheme, the correction step (5.5) can be written in matrix–vector form and then combined with the formulation (5.4) of the prediction step. This process is similar to what was done for other algorithms in Sections 4.1 and 5.1, so we omit the details. Instead, we report the results of some numerical computations of eigenvalues for some examples.

Figure 5.2 shows plots of absolute values of eigenvalues versus $k\,\Delta x$ for the two predictor–corrector schemes described above. The upper frame shows results with averaging scheme (1), and the lower frame shows results with averaging scheme (2). In this example, we assume $\Delta\tilde{p}_1/$

$\tilde{p}_2 = 0.25$, $\Delta\tilde{p}_2/\tilde{p}_2 = 0.75$, $\Delta\alpha/\alpha_2 = 0.01$, and $c_1\,\Delta t/\Delta x = 0.8$. These plots show considerable improvement over the results from the forward–backward time stepping illustrated in Fig. 4.1. Averaging scheme (2) shows better results than scheme (1). However, the predictor–corrector schemes appear not to be able to improve on the lower bound $(1 + \delta(k))^{1/2}$ that was discussed after the proof of Proposition 4.2.

Another example is graphed in Figure 4.2. Each point in the plot represents the maximum, over all k, of the absolute values of the eigenvalues for some algorithm and some value of $\Delta\alpha/\alpha_2$. As noted earlier, the small circles correspond to the forward–backward scheme discussed in Section 4. The crosses correspond to the predictor–corrector method with averaging scheme (1), and the asterisks correspond to the predictor–corrector method with averaging scheme (2). The figure suggests that the second averaging scheme may reduce the maximum growth rate from $1 + O(\sqrt{\Delta\alpha/\alpha_2})$ to $1 + O(\Delta\alpha/\alpha_2)$.

6. NUMERICAL COMPUTATIONS

We now describe the results of some numerical computations that test the analysis developed in this paper. The goal is to compare the unstable growth rates predicted by the analysis with the growth rates that are observed when the partial differential equations are solved numerically. The algorithms that are tested include the forward–backward time stepping analyzed in Section 4 and the predictor–corrector methods described in Section 5.2.

As before, we consider a linearized system in one horizontal dimension with two fluid layers. In the preceding analysis, the barotropic equations are solved exactly with respect to t, partly for the sake of simplicity and partly in order to isolate the effects of the operator splitting and baroclinic time stepping. In the present computations, we solve the barotropic equations with short time steps using a forward–backward scheme in which η is updated first and $\bar{u}$ is updated second.

Growth rates were estimated from the numerical results in the following manner. It follows from the analysis in Section 4 that each dependent variable in the solution is generally dominated by a superposition of Fourier modes of the form $\sum_{j=1}^{4} a_j \lambda_j^n e^{ikx}$, where the λ_j's are eigenvalues of the problem (4.12), the a_j's are coefficients that depend on the wavenumber k, and n is the time index. Let λ denote the maximum of $|\lambda_1|$, $|\lambda_2|$, $|\lambda_3|$, $|\lambda_4|$. For sufficiently large n, the magnitude of each Fourier mode in each dependent variable is dominated by a quantity of the form $c\lambda^n$, where c is a constant. The logarithm of this magnitude is approximately $\log c + n \log \lambda$. For each of the problem configurations described below, we plotted the logarithm of $|u'|$ in the top layer for a fixed x as a function of the time index n. The time integration was continued until the upper envelope of this graph was essentially a straight line. The graph was then used to estimate the slope $\log \lambda$ and thus λ. In the cases that yielded relatively rapid growth, the solution was computed for several thousand time steps. In other examples, it was necessary to compute for tens of thousands of time steps, or more.

In the computations described here, the velocities $\bar{u}$ and u' were taken to be sinusoidal at time $t = 0$, and the quantities η and p' were set equal to zero at $t = 0$. Solutions were computed over a finite interval in x with periodic boundary conditions. Various wavenumbers in the initial conditions were tested, and the observed growth rates as $n \to \infty$ were found to be essentially independent of wavenumber. Apparently this was due to the effects of roundoff error; over the many time steps used here, roundoff error would eventually excite the mode having the greatest growth rate, whether or not this mode was present in the initial data. This mode would then eventually dominate the solution.

Model parameters were chosen so that $\Delta\tilde{p}_1/\tilde{p}_2 = 0.25$ and $\Delta\tilde{p}_2/\tilde{p}_2 = 0.75$, and the baroclinic time step Δt was chosen so that $c_1\,\Delta t/\Delta x = 0.8$. In each computation, the barotropic equations were solved with a smaller time step Δt_f. The ratio $\Delta t/\Delta t_f$ represents the number of barotropic substeps of one baroclinic time step.

In one series of computations, the barotropic time step Δt_f was chosen so that $c_0\,\Delta t_f/\Delta x \approx 0.8$, where c_0 is the speed of external gravity waves. More precisely, Δt_f was chosen so that the ratio $\Delta t/\Delta t_f$ was the smallest integer such that $c_0\,\Delta t_f/\Delta x \le 0.8$. The results of the computations are illustrated in Fig. 6.1. The top frame shows results obtained when the forward–backward method is used to solve the baroclinic equations. The other two frames correspond to the predictor–corrector methods described in Section 5.2. In each plot, the horizontal axis represents values of $\Delta\alpha/\alpha_2$, and the vertical axis corresponds to maximum absolute values of eigenvalues. The circles represent results obtained from the analysis, and the crosses represent measurements obtained from the numerical computations. Different values of $\Delta\alpha/\alpha_2$ correspond to different values of c_0/c_1, so the ratio $\Delta t/\Delta t_f$ varies from one case to another. In most of the cases plotted in Fig. 6.1., the growth rates observed in the numerical computations are significantly larger than the rates predicted by the analysis. The results suggest that the barotropic time stepping may make a significant contribution to the growth rate.

In order to check the growth rates predicted by the analysis, additional experiments were performed with smaller values of Δt_f so as to reduce the effects of the barotropic time stepping. For one problem configuration, decreasing values of Δt_f yielded smaller growth rates until $\Delta t/\Delta t_f$ reached a value of approximately 1000, and the growth rates then remained essentially constant as Δt_f was reduced further. A series of computations was then per-

formed with $\Delta t/\Delta t_f = 10{,}000$, and the results are shown in Fig. 6.2. In this case the growth rates measured from the numerical computations agree closely with the rates predicted by the analysis.

7. SUMMARY AND CONCLUSIONS

In a numerical model of ocean circulation, it is highly desirable to split the fast external motions and slow internal motions into separate subproblems. However, if the splitting is inexact, then the equations that are intended to model the slow motions may actually admit some fast motions. This could create stability problems if these equations are advanced in time with an explicit method having a long time step. In this paper, one example of a splitting is applied to a simple physical situation consisting of a linearized flow in one horizontal dimension with two fluid layers and flat bottom topography. When some standard methods are used to discretize the slow equations, the resulting algorithms are unstable. In a more realistic ocean model, mode mixing could also be generated by nonlinearity and variable topography. Numerical ocean models typically contain dissipative mechanisms of various types, and these may aid in suppressing the effects of inexact splitting. It would be valuable to analyze and construct splittings so as to minimize the use of such mechanisms, especially for long-term integrations such as those found in climate modeling. This problem is the subject of current research.

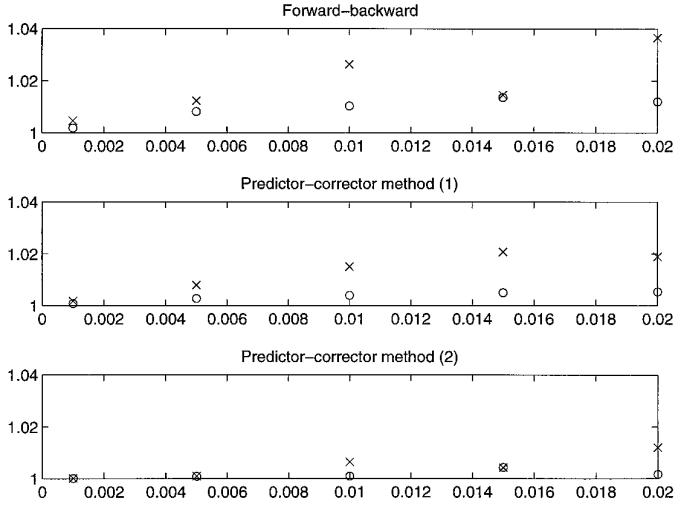

FIG. 6.1. Comparison of growth rates predicted by the analysis with growth rates observed in numerical solutions of the partial differential equations. The model parameters and the axes are the same as in Fig. 4.2. In each of the numerical solutions, the time step Δt_f for the barotropic equations is chosen so that $c_0\ \Delta t_f/\Delta x \approx 0.8$. In each frame, the circles represent the maximum absolute values of eigenvalues as determined from the analysis in this paper. The crosses represent measurements from numerical solutions. In the analysis, the barotropic equations are solved exactly with respect to t, and the discrepancies between the results shown here are due primarily to the time discretization of the barotropic equations when the system is solved numerically.

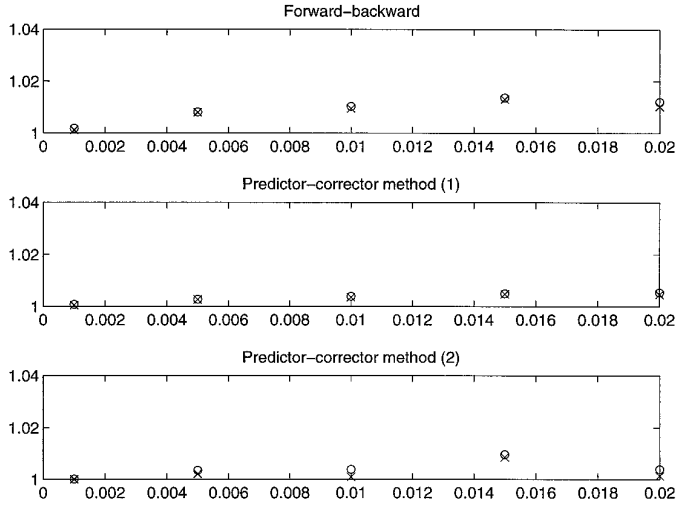

FIG. 6.2. Comparison of growth rates. The situation is the same as in Fig. 6.1, except that the numerical solutions of the system are based on much smaller time steps Δt_f for the barotropic equations. In the present case, the discretization errors for the barotropic equations are much smaller, and the numerical results agree closely with the results of the analysis.

ACKNOWLEDGMENTS

We thank Rainer Bleck, Linda Smith, Roland de Szoeke, and Len Margolin for useful conversations regarding various matters discussed in this paper. We also thank Boon Chua for performing the numerical computations described in Section 6. Higdon's work was supported by National Science Foundation Grant DMS-9103197. Bennett's work was supported by Office of Naval Research Grant N00014-93-1-0422.

REFERENCES

1. A. F. Bennett, *Inverse Methods in Physical Oceanography* (Cambridge Univ. Press, Cambridge, UK, 1992).
2. R. Bleck and L. T. Smith, *J. Geophys. Res. C* **95,** 3273 (1990).
3. A. F. Blumberg and G. L. Mellor, ''A Description of a Three-Dimensional Coastal Ocean Circulation Model,'' in *Three-dimensional Coastal Ocean Models,* edited by N. Heaps (Am. Geophys. Union, Washington, DC, 1987), p. 1.
4. K. Bryan, *J. Comput. Phys.* **4,** 347 (1969).
5. M. D. Cox, GFDL Ocean Group Technical Report No. 1, Geophysical Fluid Dynamics Laboratory, Princeton, NJ, 1984 (unpublished).
6. R. A. de Szoeke and A. F. Bennett, *J. Phys. Oceanogr.* **23,** 2254 (1993).
7. J. K. Dukowicz and R. D. Smith, *J. Geophys. Res. C* **99,** 7991 (1994).
8. A. Eliassen and E. Kleinschmidt, ''Dynamic Meteorology,'' in *Handbuch der Physik,* Vol. 48, edited by S. Flügge (Springer-Verlag, Berlin, 1957), p. 1.
9. A. E. Gill, *Atmosphere–Ocean Dynamics* (Academic Press, San Diego, CA, 1982).
10. G. J. Haltiner and R. T. Williams, *Numerical Prediction and Dynamic Meteorology* (Wiley, New York, 1980).

11. P. D. Killworth, D. Stainforth, D. J. Webb, and S. M. Paterson, *J. Phys. Oceanogr.* **21,** 1333 (1991).
12. P. M. Morse and H. Feshbach, *Methods of Theoretical Physics* (McGraw–Hill, New York, 1953).
13. J. M. Oberhuber, *J. Phys. Oceanogr.* **23,** 808 (1993).
14. J. Pedlosky, *Geophysical Fluid Dynamics,* 2nd ed. (Springer-Verlag, New York, 1987).
15. O. M. Phillips, *The Dynamics of the Upper Ocean* (Cambridge Univ. Press, Cambridge, UK, 1966).
16. M. H. Redi, *J. Phys. Oceanogr.* **12,** 1154 (1982).
17. R. D. Richtmyer and K. W. Morton, *Difference Methods for Initial Value Problems,* 2nd ed. (Interscience, New York, 1967).
18. A. R. Robinson (Ed.), *Eddies in Marine Science* (Springer-Verlag, Berlin, 1983).
19. A. J. Semtner and R. M. Chervin, *J. Geophys. Res.* **93,** 15502 (1988).
20. A. J. Semtner and R. M. Chervin, *J. Geophys. Res.* **97,** 5493 (1992).
21. R. D. Smith, J. K. Dukowicz, and R. C. Malone, *Physica D* **60,** 38 (1992).